LBL-23341 c.2
Preprint

Lawrence Berkeley Laboratory

UNIVERSITY OF CALIFORNIA

Physics Division

1987

DOCUMENTS SECTION

Mathematics Department

To be submitted for publication

A STUDY OF THE VORTEX STREET METHOD AND ITS RATE OF CONVERGENCE

E.G. Puckett

April 1987

TWO-WEEK LOAN COPY

This is a Library Circulating Copy which may be borrowed for two weeks.

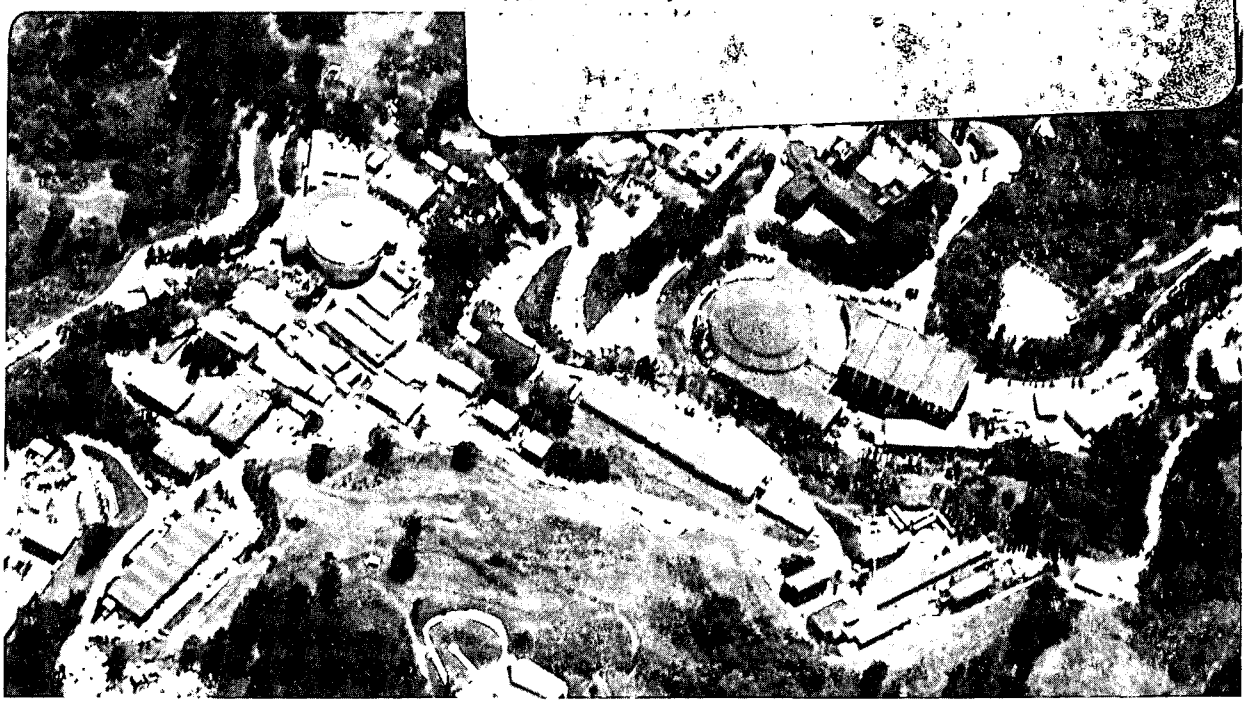

LBL-23341 c.2

Prepared for the U.S. Department of Energy under Contract DE-AC03-76SF00098

DISCLAIMER

This document was prepared as an account of work sponsored by the United States Government. While this document is believed to contain correct information, neither the United States Government nor any agency thereof, nor the Regents of the University of California, nor any of their employees, makes any warranty, express or implied, or assumes any legal responsibility for the accuracy, completeness, or usefulness of any information, apparatus, product, or process disclosed, or represents that its use would not infringe privately owned rights. Reference herein to any specific commercial product, process, or service by its trade name, trademark, manufacturer, or otherwise, does not necessarily constitute or imply its endorsement, recommendation, or favoring by the United States Government or any agency thereof, or the Regents of the University of California. The views and opinions of authors expressed herein do not necessarily state or reflect those of the United States Government or any agency thereof or the Regents of the University of California.

LBL-23341

A STUDY OF THE VORTEX STREET METHOD AND ITS RATE OF CONVERGENCE[1]

Elbridge Gerry Puckett[2]

Department of Mathematics
and
Lawrence Berkeley Laboratory
University of California
Berkeley, California 94720

April 1987

[1]Supported in part by the Applied Mathematical Sciences Subprogram of the Office of Energy Research, U.S. Department of Energy under contract DE-AC03-76SF00098.

[2]Current address: Lawrence Livermore National Laboratory, Livermore, CA 94550.

A Study of the Vortex Sheet Method and Its Rate of Convergence

Elbridge Gerry Puckett †

U. C. Berkeley Mathematics Department ‡
and Lawrence Berkeley Laboratory
Berkeley, California 94720

ABSTRACT

We study Chorin's vortex sheet method used to solve the Prandtl boundary layer equations and to impose the no-slip boundary condition in the random vortex method solution of the Navier-Stokes equations. This is a particle method in which the particles carry concentrations of vorticity and undergo a random walk to approximate the diffusion of vorticity in the boundary layer. A spline 'smoothing' is presented which results in a smoother velocity field and in the no-slip boundary condition being satisfied to higher order. It is shown that the particle creation algorithm and the random walk taken together provide a consistent approximation to the heat equation. In particular it is shown that in the L^1 norm the consistency error is $O\left((h + \omega_{\max})\sqrt{\nu\Delta t}\right)$ where h is the sheet length, $\omega_{\max}$ is the maximum sheet strength, Δt is the time step and ν is the viscosity. We demonstrate numerically that the method converges in the case of Blasius flow and establish rates of convergence in terms of the computational parameters. This numerical study reveals that errors grow when the sheet length tends to 0 much faster than the maximum sheet strength. Finally, we present the results of computer experiments with spline smoothing, second order time discretization, and sheet tagging.

Keywords : boundary layer equations, particle method, random vortex method, random walk, vorticity

AMS Subject Classification : 35, 60, 65, 76

---

† This work was supported in part by the Applied Mathematical Sciences Subprogram of the Office of Energy Research, U.S. Department of Energy under contract DE-AC03-76SF00098, in part by the Office of Naval Research under contract N00014-76-C-0316 and is a portion of the author's PhD dissertation in the U. C. Berkeley Mathematics Department.

‡ Current address: Lawrence Livermore National Laboratory, Livermore, CA 94550

1. The Prandtl Equations

The vortex sheet method is a numerical method, due to Chorin [9], for solving the Prandtl boundary layer equations ([10, 20, 24, 31],

$$u_t + uu_x + vu_y = -p_x + \nu u_{yy} \tag{1.1a}$$

$$u_x + v_y = 0 \tag{1.1b}$$

subject to the boundary conditions

$$u(x,0,t) = 0 \tag{1.1c}$$

$$v(x,0,t) = 0 \tag{1.1d}$$

$$\lim_{y\to\infty} u(x,y,t) = U_\infty(x,t)\,. \tag{1.1e}$$

Here u is the velocity component in the x direction, v the component in the y direction, p the pressure, ν the kinematic viscosity, and $U_\infty(x,t)$ the free stream velocity. U_∞ is independent of y and assumed to be known. We assume a flow with constant density $\rho \equiv 1$.

Equations (1.1a-e) are derived from the Navier-Stokes equations under the assumption that the velocity component perpendicular to the boundary is small relative to the tangential component. They are valid for general flows along curved walls as long as the boundary-layer thickness is small compared to the wall's radius of curvature (see White [31], p. 256, Cheer [5]). Both the boundary layer equations and the vortex sheet method may be generalized to three dimensions (Chorin, [11]). For simplicity we work in two dimensions and assume that the boundary is a flat wall of length L, beginning at $(a,0)$ and extending to $(b,0)$.

1.1. The Vorticity Formulation of the Prandtl Equations For solutions of the boundary layer equations the vorticity is given by $\omega = -u_y$ ([10], p. 100). Differentiating equation (1.1a) with respect to y and recalling that in the boundary layer the pressure, p, is independent of y (see White [31], p. 254) we obtain the vorticity formulation of Prandtl equations

$$\frac{D\omega}{Dt} = \nu\,\omega_{yy} \tag{1.2a}$$

$$\omega = -u_y \tag{1.2b}$$

$$u_x + v_y = 0 \tag{1.2c}$$

where $\frac{D}{Dt} = \partial_t + u\,\partial_x + v\,\partial_y$ is the material derivative.

This equation will be useful in understanding the vortex sheet method. Note that equation (1.2a) consists of two evolution equations: a *convection equation*,

$$\frac{D\omega}{Dt} = 0 \tag{1.3}$$

and a *diffusion equation*,

$$\omega_t = \nu\,\omega_{yy}\ . \tag{1.4}$$

In particular, note that for solutions of (1.3) vorticity is constant on particle paths. The advection step in the vortex sheet method is based on the principle that for solutions of the inviscid Prandtl equations vorticity is constant on particle paths.

2. The Vortex Sheet Method

The vortex sheet method is a fractional step method in which equation (1.3) is solved in one step and equation (1.4) in the other, with the vorticity field obtained at the end of one step being used as the initial data for the next. The method was designed in the spirit of the random vortex method, [8]. It is a particle method. The particles carry concentrations of vorticity and the velocity field is reconstructed from the particle positions.

The solution of (1.3) is obtained by convecting the particles according to the velocity field. Equation (1.4) is solved by allowing the particles to undergo a random walk in the y direction. During the random walk solution of (1.4) particles are created at the wall to ensure that the BC (1.1c) is satisfied. This creation of particles mimics the physical creation of vorticity at the wall.

2.1. Notation Before describing the details of the method we introduce some notation. Let $P_{\Delta t}\, u^0$ denote the solution at time $t = \Delta t$ of the Prandtl equations (1.1a-e) with initial data $u^0(x, y) = u(x, y, 0)$. Similarly, let $A_{\Delta t}\, u^0$ denote the solution at $t = \Delta t$ of the inviscid equation

$$\frac{Du}{Dt} = -p_x \tag{2.1a}$$

$$u_x + v_y = 0 \tag{2.1b}$$

$$u(x, \infty, t) = U(x), \qquad t > 0, \tag{2.1c}$$

$$v(x, 0, t) = 0, \qquad t > 0, \tag{2.1d}$$

with initial data u^0 and let $D_{\Delta t}\, u^0$ be the solution of the diffusion equation

$$u_t = \nu u_{yy} \tag{2.2a}$$

$$u(x,0,t) = 0, \qquad t > 0, \tag{2.2b}$$

with initial data u^0.

The vortex sheet method consists of finding approximations $\widetilde{A}_{\Delta t}$ and $\widetilde{D}_{\Delta t}$ to the solution operators $A_{\Delta t}$ and $D_{\Delta t}$ and then using $\widetilde{D}_{\Delta t}\widetilde{A}_{\Delta t}\, u^0$ as an approximation to $P_{\Delta t}\, u^0$. We write the vortex sheet approximation to the solution, $u^k = (P_{\Delta t})^k\, u^0$, of (1.1a-e) at time $t = k\,\Delta t$ with initial data u^0 as

$$\tilde{u}^k = (\widetilde{D}_{\Delta t}\widetilde{A}_{\Delta t})^k\, u^0 \ .$$

We will usually use $\tilde{u}$ to denote an approximation to u , $\tilde{\omega}$ an approximation to ω, etc.

2.2. The Approximate Velocity Field One feature common to all vortex methods is that the velocity field $(u\,,v)$ is recovered from the vorticity ω. From (1.2b) we have

$$u(x,y) = U(x) + \int_y^\infty \omega(x,y')\, dy' \ . \tag{2.3}$$

In the vortex sheet method we replace the integral on the right hand side by a sum,

$$\tilde{u}(x,y) = U(x) + \sum_j \omega_j\, b_h(x - x_j)\mathrm{H}(y_j - y), \tag{2.4}$$

where $\mathrm{H}(y)$ is the Heaviside function,

$$\mathrm{H}(y) = \begin{cases} 0, & x < 0\,, \\ 1, & x \geq 0\,. \end{cases} \tag{2.5}$$

The function b_h, known as the *cutoff* or *smoothing* function, is defined by

$$b_h(x) = b(x/h) \tag{2.6}$$

where b can be chosen in several ways. In [9] Chorin used

$$b(x) = \begin{cases} 1 - |x|, & \textit{if } |x| \leq 1 \\ 0, & \textit{otherwise.} \end{cases} \tag{2.7}$$

The cutoffs $b_h(x - x_j)$ with b as in (2.7) are frequently referred to as 'hat' functions. (Tiemroth [30] refers to them as 'tent' functions.) One of the purposes of this work is to suggest alternate choices for b. We will discuss these and other smoothing functions in Chapter 3 below.

All cutoffs that we consider will be normalized so that

$$b(0) = 1 \tag{2.8a}$$

and have compact support,

$$b(x) = 0, \qquad \text{for } |x| \geq R\,. \tag{2.8b}$$

Typically, $R = 1$ or $R = 2$.

Each term of the sum in (2.4) is referred to as a *vortex sheet*. The jth sheet has center (x_j, y_j) and *strength*, or *weight*, ω_j. By (2.8b) each sheet has length $2Rh$ where R depends on the particular smoothing function chosen. From (2.4) we see that for fixed x the difference between $\bar{u}$ at a point immediately above the jth sheet and $\bar{u}$ at a point immediately below it is $\omega_j\ b_h(x - x_j)$. This jump in the tangential velocity as one crosses the line $y = y_j$ is the motivation for referring to each computational element as a 'vortex sheet'.

From (2.4) we have

$$\tilde{u}(x,y) = U(x) + \int_y^\infty \sum_j \omega_j \; b_h(x - x_j)\, \delta(y_j - y')\, dy', \tag{2.9}$$

where δ is the Dirac delta function. Thus, our approximation to the vorticity is

$$\tilde{\omega}(x,y) = \sum_j \omega_j \, b_h(x - x_j)\, \delta(y_j - y), \tag{2.10}$$

and we see that each sheet carries a linear concentration of vorticity which varies like $b_h(x - x_j)$ as one moves along the line segment $(-Rh \le x - x_j \le Rh\,,\; y = y_j)$.

Given the horizontal velocity u we can recover the vertical velocity with the aid of equation (1.1b),

$$v(x,y) = -\int_0^y u_x(x,y')\, dy' \,. \tag{2.11}$$

Our approximation $\tilde{v}$ of the vertical velocity is therefore

$$\begin{aligned} \tilde{v}(x,y) &= -\int_0^y \partial_x \tilde{u}(x,y')\, dy' \\ &= -U_x(x)\, y - \partial_x \sum \omega_j \; b_h(x - x_j) \int_0^y \mathrm{H}(y_j - y')\, dy' \qquad (2.12) \\ &= -U_x(x)\, y - \sum \omega_j \; \partial_x \; b_h(x - x_j)\, \min(y, y_j) \,. \end{aligned}$$

Thus, if $b(x)$ is C^1, then

$$\tilde{v}(x,y) = -U_x(x)\, y - \sum \omega_j \; h^{-1}\, b_h'(x - x_j)\, \min(y, y_j) \tag{2.13}$$

where $b_h' = b'(x/h)$. On the other hand, if b is not differentiable everywhere (this is the case for the hat functions in (2.7)), one can use a divided difference approximation to b_h',

$$\tilde{v}(x,y) = -U_x(x)\,y - \sum \omega_j\, h^{-1}\left(b_h\left(x + \frac{h}{2} - x_j\right) - b_h\left(x - \frac{h}{2} - x_j\right)\right) \min(y, y_j)\,. \quad (2.14)$$

This is the most commonly used version. In Chapter 3 we propose cutoffs that are C^p for $p \geq 1$ thereby enabling one to use the exact derivative in (2.13). This is easier to program and presumably more accurate than using divided differences.

2.3. Integration of the Equations in Time Note that our approximation, $(\tilde{u}, \tilde{v})$, to the velocity field (u, v) is completely determined by the positions of the particles (x_j, y_j) and their weights ω_j. (We will use the words 'sheets' and 'particles' interchangeably.) We denote the time step by Δt, the position of the jth particle at the kth time step by (x_j^k, y_j^k) and the velocity field derived from these positions by $(\tilde{u}^k, \tilde{v}^k)$. Given this velocity field the velocity field at the next time step, $(\tilde{u}^{k+1}, \tilde{v}^{k+1})$, is determined as follows.

2.3.1. The Advection Step Given $(\tilde{u}^k, \tilde{v}^k)$ our approximation to the solution of the advection equation (2.1a-c) is found by moving the sheets according to

$$x_j^{k+1/2} = x_j^k + \Delta t\;\tilde{u}^k(x_j^k, y_j^k) \quad (2.15a)$$

$$y_j^{k+1/2} = y_j^k + \Delta t\;\tilde{v}^k(x_j^k, y_j^k) \quad (2.15b)$$

Thus, the velocity field after the first of the two fractional steps is

$$\tilde{u}^{k+1/2}(x,y) = U(x) + \sum_j \omega_j\; b_h(x - x_j^{k+1/2})\,\mathrm{H}(y_j^{k+1/2} - y), \quad (2.16a)$$

$$\tilde{v}^{k+1/2}(x,y) = -U_x(x)\,y - \sum_j \omega_j\;\partial_x b_h(x - x_j^{k+1/2}) \min(y, y_j^{k+1/2})\,. \quad (2.16b)$$

Note that $\omega^{k+1/2} \equiv -\partial_y \tilde{u}^{k+1/2}$ approximates the solution of (1.3) with initial data $\tilde{\omega}^k = -\partial_y \tilde{u}^k$ in the sense that vorticity is constant on approximate particle paths $(x_j^k, y_j^k) \rightarrow (x_j^{k+1/2}, y_j^{k+1/2})$. In the notation of §2.1 we write

$$\tilde{u}^{k+1/2} = \widetilde{A}_{\Delta t} \tilde{u}^k \ .$$

Note that (2.15a,b) is the Euler's method solution of the ODE's

$$\frac{dx_j}{dt} = u(x_j, y_j, t), \tag{2.17a}$$

$$\frac{dy_j}{dt} = v(x_j, y_j, t), \tag{2.17b}$$

where we approximate $u(x, y, k\Delta t)$ by $\tilde{u}^k(x, y)$ and $v(x, y, k\Delta t)$ by $\tilde{v}^k(x, y)$. One can choose to solve (2.17a,b) with a higher order ODE solver. The use of higher order ODE solvers in the vortex method solution of the inviscid Navier-Stokes equations have been studied in [1] and [17] but to date there has been no theoretical work done on the use of a higher order solution of (2.17a,b) for the vortex sheet method. In Chapter 6 we will present the results of a numerical experiment to compare a second order solution of (2.17a,b) with the first order solution given by (2.15a,b).

2.3.2. The Particle Creation and Diffusion Step The second part of the splitting procedure is the random walk solution of (2.2a,b) with initial data $\tilde{u}^{k+1/2}$. This consists of creating sheets at grid points on the wall in order to satisfy the no-slip boundary condition and letting all sheets undergo a random walk, with reflection, in the y direction.

Choose h so that the wall length, L, is an integral multiple of h, $L = r\ h$. Pick points $a_1, \ldots, a_r$ on the wall so that $a_1 = \frac{h}{2}$, $a_i - a_{i-1} = h$, $i = 2, \ldots, r$, and $a_r = L - \frac{h}{2}$. We approximate the boundary condition (1.1c) by requiring that at the end of every time step

the tangential velocity at the wall *approximately* satisfy

$$\tilde{u}(a_i,0) = 0, \qquad i = 1, \ldots, r. \tag{2.18}$$

In other words, for some small parameter, $\omega_{\min}$, we require that $\tilde{u}$ satisfy

$$|\tilde{u}(a_i,0)| \leq \omega_{\min}, \qquad i = 1, \ldots, r \tag{2.19}$$

at the end of every time step. This is accomplished in the following manner.

Let $\omega_{\max}$ denote a computational parameter called the *maximum sheet strength*. All sheet strengths will be chosen so that $|\omega_j| \leq \omega_{\max}$. As we shall see in Chapter 4, $\omega_{\max}$ is the computational parameter which most directly influences the accuracy of the random walk. After the advection step the tangential velocity, $\tilde{u}^{k+1/2}$, will in general fail to satisfy (2.19), even if the velocity at the previous time step, $\tilde{u}^k$, does. Let $u_i = \tilde{u}^{k+1/2}(a_i,0)$. At each a_i we create $q_i \geq 0$ sheets, with center $(x_i, y_i) = (a_i, 0)$ and strength ω_{il}, so that for $j = 1, \ldots, r$,

$$\left| \tilde{u}^{k+1/2}(a_j,0) + \sum_{i=1}^{r} \sum_{l=1}^{q_i} \omega_{il}\, b_h(a_j - x_i)\, \mathrm{H}(y_i - 0) \right| = \left| u_j + \sum_{i=1}^{r} \sum_{l=1}^{q_i} \omega_{il}\, b_h(a_j - a_i) \right|$$

$$\leq \omega_{\min}.$$

We assume that for a given i the ω_{il} are all equal and will often write ω_i rather than ω_{il}.

One has considerable leeway when choosing q_i and ω_i. We will therefore discuss this aspect of the algorithm in greater detail. We begin by describing the version originally proposed by Chorin in [9]. We then present a variation on his idea which leads to fewer sheets at the expense of satisfying (2.18) less accurately. In §6.7 we report on a numerical experiment in which we find that both particle creation algorithms produce comparable errors.

Assume that $R = 1$ in (2.8b). Hence,

$$b_h(a_i - a_j) = \delta_{ij}$$

where δ_{ij} is the Kronecker delta function. This is the case for Chorin's cutoff (2.7). In Chapter 3 below we will remove this assumption and describe a variation on the creation algorithm.

Particle Creation Algorithm A In this version a sheet is created at a_i if $|u_i| \geq \omega_{\min}$ where $\omega_{\min} < \omega_{\max}$. For example, $\omega_{\min}$ might be chosen to be on the order of the computer's roundoff error. Let $[x]$ denote the greatest integer less than or equal to x. If $|u_i| \geq \omega_{\min}$, then we create

$$q_i = \begin{cases} |u_i| / \omega_{\max} & \textit{if } \omega_{\max} \textit{ divides } u_i \textit{ evenly} \\ [\,|u_i| / \omega_{\max} + 1] & \textit{otherwise} \end{cases}$$

sheets at $(a_i, 0)$, each of strength $\omega_i = -u_i / q_i$. Otherwise we set $q_i = 0$ and create no new sheets at $(a_i, 0)$.

As we shall see presently, the random walk does not alter the tangential velocity at the wall. Thus, the tangential velocity at time $t = (k+1)\Delta t$ satisfies

$$|\tilde{u}^{k+1}(a_i, 0)| = |u_i + \sum_{l=1}^{q_i} \omega_i| = |u_i + q_i \omega_i| \leq \begin{cases} 0, & \text{if } q_i > 0, \\ \omega_{\min}, & \text{if } q_i = 0. \end{cases}$$

Thus, the approximate BC (2.18) is either satisfied exactly or with an error which is $O(\omega_{\min})$.

Particle Creation Algorithm B An alternate version of this particle creation algorithm was used in [7, 29, 30] as well as in the present work. Let $q_i = [\,|\,u_i\,|\,/\omega_{\max}]$. At the ith grid point we create q_i sheets, each with strength $\omega_i = -\,sign\,(u_i)\,\omega_{\max}$ and center $(a_i,0)$. Our approximation to the tangential velocity at time $t = (k+1)\Delta t$ now satisfies

$$|\,\tilde{u}^{k+1}(a_i,0)\,| = |\,u_i + \sum_{l=1}^{q_i}\omega_i\,| = |\,u_i - q_i\,sign\,(u_i)\,\omega_{\max}\,| < \omega_{\max}\,. \tag{2.20}$$

Thus, the approximate BC (2.18) is satisfied somewhat less accurately than in Algorithm A. However, our experience has been that this has a negligible effect on the overall accuracy of the solution. In Chapter 4 we will present some analysis which clarifies the relationship between the accuracy with which we approximate the no-slip boundary condition and the overall error in the random walk solution of (2.2a,b). In Chapter 6 we present numerical results that indicate Algorithm B creates fewer sheets without any noticeable deterioration in the accuracy of the computed solution.

We remark that Algorithm B is essentially Algorithm A with $\omega_{\min} = \omega_{\max}$ except that in Algorithm B all sheet strengths are of equal magnitude, $\omega_{\max}$. This is similar to the algorithm studied in [16]. We believe that creating all sheets with the same strength gives one better control over the variance of the solution while simultaneously creating fewer sheets, thereby producing a more cost efficient algorithm.

Now let every sheet including those just created take a random walk in the y direction, reflecting those sheets which go below the wall. The new particle positions are given by

$$x_j^{k+1} = x_j^{k+1/2} \tag{2.21a}$$

$$y_j^{k+1} = |\,y_j^{k+1/2} + \varsigma_j\,| \tag{2.21b}$$

where ς_j is a Gaussian distributed random number with mean 0 and variance $2\nu\Delta t$. The velocity field at time $t = (k+1)\Delta t$ is thus

$$\tilde{u}^{k+1}(x,y) = U(x) + \sum_{j=1}^{N_k} \omega_j \; b_h(x - x_j^{k+1/2})\, \mathrm{H}(\,|\, y_j^{k+1/2} + \varsigma_j \,|\, - y\,)$$

$$+ \sum_{i=1}^{r} \sum_{l=1}^{q_i} \omega_i \; b_h(x - a_i)\, \mathrm{H}(\,|\, \varsigma_{il} \,|\, - y\,) \tag{2.22}$$

$$= U(x) + \sum_{j=1}^{N_{k+1}} \omega_j \; b_h(x - x_j^{k+1})\, \mathrm{H}(y_j^{k+1} - y\,)$$

where $\sum_{j=1}^{N_k}$ indicates that the sum is over those sheets that existed in the flow at the kth time step while $\sum_{j=1}^{N_{k+1}}$ is over all sheets, new and old, that exist at the end of the $k+1$st time step. Using the notation introduced in §2.1 we write

$$\tilde{u}^{k+1} = \widetilde{D}_{\Delta t}\, \tilde{u}^{k+1/2}\,.$$

It is appropriate to make several remarks here. In §4.2 we will prove that

$$D_{\Delta t}\, \tilde{u}^{k+1/2}(x,y) = \mathrm{E}\,[\, \widetilde{D}_{\Delta t}\, \tilde{u}^{k+1/2}(x,y)\,] + \mathrm{O}(h + \omega_{\max}) \tag{2.23}$$

where the expected value is only over those random walks taken at this time step. In other words, the expected value of the sheet creation and random walk process applied to $\tilde{u}^{k+1/2}$ differs from the exact solution to (2.2a,b) with initial data $\tilde{u}^{k+1/2}$ by an error which is $\mathrm{O}(h + \omega_{\max})$. This error is due to our failure to satisfy the no slip boundary condition exactly. In fact, if the new sheets are chosen so that (2.18) is satisfied exactly at a_i, then we have

$$D_{\Delta t}\, \tilde{u}^{k+1/2}(a_i,y) = \mathrm{E}\,[\, \widetilde{D}_{\Delta t}\, \tilde{u}^{k+1/2}(a_i,y)\,]\,.$$

This has several implications. In the original version of the vortex sheet method Chorin created twice as many sheets as needed, whose total was twice that needed to cancel the velocity at the wall ([9], p. 423). He then let these new sheets random walk *without reflection* throwing away those sheets that went below the wall. (Of course the other sheets were random walked, with reflection, as above.) In a more recent version ([11], p. 6) Chorin again created twice as many sheets as needed but this time employed a rejection technique to ensure that exactly half of these sheets took their random walk in the positive y direction. Equation (2.23) tells us that these special procedures are unnecessary. It is sufficient to create sheets as in Algorithms A or B above and allow them to undergo a random walk with reflection.

The results mentioned above also indicate that the sheet creation and the random walk are part of the same process. That is, they are one step in a two step fractional step method (the advection step being the other) rather than being two separate steps in a three step fractional step method. Furthermore, the new sheets should undergo a random walk just as the old ones do, without waiting a time step before diffusing them from the wall.

2.4. Sheet Tagging In [9] Chorin proposed the following 'variance reduction technique'. During the sheet creation process each sheet is assigned a positive integer, called a *tag*, as follows. Let T_k be the last tag assigned at the k th time step. Then, during the $k+1$st time step, the first sheet created at every grid point is assigned the number T_k+1, the second sheet is assigned T_k+2, and so on until all sheets have a tag. Thus, no two sheets created at the same grid point will have the same tag while one sheet at each grid point will have the same tag (except, of course, when more sheets need to be created at one grid point than another). When the sheets are random walked all sheets with the same tag get assigned the same random walk.

The motivation behind this procedure is twofold. First, if one uses the vortex sheet method to model flow past an infinite plate with constant free stream velocity ([10], pp. 92-95),

then with sheet tagging the vortex sheet method reduces to the random walk solution of the heat equation. This eliminates all error due to the advection step. Second, on heuristic grounds it is believed that vorticity leaving the wall diffuses at the same rate everywhere along the wall and it was thought that the sheet tagging mimicked this process.

Our experience has been that, with the exception of the infinite flat plate problem, sheet tagging has at best a benign influence on the accuracy of the vortex sheet method. Numerical experiments show that for problems in which sheets with the same tag tend to overlap the tagging procedure leads to an increase in both the expected value and the variance of the error. In §6.8 we present the results of one such experiment. We also address this issue from an analytical point of view in the remarks after the proof of Theorem 4.6.

3. Smoothing

We now turn to a discussion of the smoothing function, b_h. Let us begin by considering the smoothness of our approximation as a function of y. From (2.4) it is apparent that, for each fixed x, the approximation $\tilde{u}^k(x,y)$ is a step function in y. This is analogous to the random gradient method. In both cases it is natural to inquire what happens if one uses something smoother than a step function.

In unpublished work the author replaced the step function approximation described in §2.1 of [21] by a piecewise linear function and used it to compute the traveling wave solution described in §9.1 of [21]. The piecewise linear version produced a significantly better approximation to the initial data at time $t = 0$. After several time steps, however, the error was comparable to that incurred by the original method. This is due to the following reason: for fixed t the accuracy in approximating a function on $\mathbb{R}$ by a step function is $O(N^{-1})$ where N is the number of particles (jumps in the function). When one uses a higher order approximation this accuracy improves. This accounts for the observed decrease in the initial error. On the other hand, the error due to solving the diffusion equation by random walking the particles is $O(\sqrt{N}^{-1})$ (see [16, 21, 22]). Consequently, any accuracy attained through the use of a higher order spacial approximation is quickly lost by the random walk.

Now fix $x = x_0$ in (2.4) and consider the approximation $\tilde{u}^k(x_0,y)$ to the one dimensional slice of the tangential velocity, $u(x_0,y,k\Delta t)$. Because of the similarity between this approximation and the random gradient approximation it is plausible that making $\tilde{u}^k$ smoother as a function of y (i.e., replacing $H(y_j - y)$ in (2.4) by something smoother) would not result in an overall improvement in the accuracy of the method. To the author's knowledge all versions of the vortex sheet method currently in use employ a step function approximation to u as a function of y.

3.1. Piecewise Constant Cutoffs (No Smoothing) Given the above considerations it is natural to conclude that smoothing in the x direction will lead to little or no improvement as well. For example, one might to choose a cutoff of the form $b(x) = s(x)$ where s is defined by

$$s(x) = \mathrm{H}(\tfrac{1}{2} - |x|) . \tag{3.1}$$

Here we have chosen the support of s to be of length one in order to satisfy the requirement that the total circulation around a sheet of length h and unit weight must be h. Furthermore, assuming that we have an equally spaced grid on the wall, with spacing h, it is apparent that the desire to satisfy (1.1c) as best possible leads to choosing sheets of length h.

It has been observed that the vortex sheet method performs poorly when this cutoff is used. We offer the following explanation. For $b(x) = s(x)$ the tangential velocity $\tilde{u}$ is piecewise constant as a function of x. Consequently, our approximation to the derivative $\partial_x \tilde{u}$ in (2.14) is poor. This in turn leads to large errors in the particle paths through (2.15b). To rectify this problem Chorin proposed using a piecewise linear approximation to u. We now turn to a discussion of his cutoff.

3.2. Piecewise Linear Smoothing It is apparent from (2.4) that the degree to which $\tilde{u}$ is differentiable as a function of x is completely determined by the differentiability of b_h. (We always assume that $U(x)$ is at least as smooth as b_h.) For example, to obtain an approximation which is piecewise linear in x one may use $b(x) = l(x)$ where

$$l(x) \equiv \begin{cases} 1 - |x|, & \textit{if } |x| \leq 1 \\ 0, & \textit{otherwise.} \end{cases} \tag{3.2}$$

This cutoff was first used by Chorin [9]. In fact, with the exception of the present work, to the author's knowledge it is the only cutoff in use. It has been used successfully for a wide variety of problems, usually in conjunction with some variant of the random vortex method.

For example, see Cheer [5, 6], Ghoniem, Chorin and Oppenheim [13], Ghoniem and Sethian [29], Sethian [27, 28], and Tiemroth [30].

For $b(x) = l(x)$ the approximate tangential velocity, $\tilde{u}$, is only piecewise C^1, failing to be differentiable at $x = x_j$ and $x = x_j \pm h$ for each j. Therefore, one must still use a divided difference approximation to the derivative $\partial_x b_h(x)$ as in (2.14). In §6.5 we report on the results of a numerical experiment to compare this approximation to a version in which $\tilde{u}$ is C^2 as a function of x.

It is instructive to examine this smoothing process from another perspective. At each time step we would ideally like to create sheets at the wall so that the computed solution satisfies the boundary condition (1.1c),

$$\tilde{u}^{k+1}(x,0) = 0$$

for all $x \in [a,b]$. Define

$$g(x) \equiv \tilde{u}^{k+1/2}(x,0) .$$

The velocity field, $\tilde{u}_{opt}^{k+1}$, defined by

$$\tilde{u}_{opt}^{k+1}(x,y) \equiv U(x) + \sum \omega_j \; b_h(x - x_j^{k+1}) \, H(\,|\, y_j^{k+1/2} + \varsigma_j \,| - y) - g(x)\,\mathrm{H}(\,|\,\varsigma\,| - y)$$

where ς and the ς_j are independent Gaussian distributed random variables with mean 0 and variance $2\nu\Delta t$ is the optimal choice for $\tilde{u}^{k+1}$ since $\tilde{u}_{opt}^{k+1}$ satisfies

$$\mathrm{E}\,[\,\tilde{u}_{opt}^{k+1}(x,y)\,] = D_{\Delta t}\,\tilde{u}^{k+1/2}(x,y),$$

for *all* $x \in [a,b]$. (This is Theorem 4.1.) In particular, $\tilde{u}_{opt}^{k+1}(x,0) = 0$ for all x on the wall.

However, we wish to write $\tilde{u}^{k+1}$ as the sum of vortex sheets. Therefore, our task is to find ω_{il} such that

$$\tilde{g}(x) \equiv -\sum_{i=1}^{r} \sum_{l=1}^{q_i} \omega_{il}\ b_h(x-a_i) = \sum_{i=1}^{r} u_i^l\ b_h(x-a_i) \tag{3.3}$$

is the best possible approximation to g. For $b_h(x) = l(x/h)$ where l is defined by (3.2) this amounts to finding a piecewise linear interpolant for g, i.e., a first order spline. In fact, for this choice of smoothing the functions

$$b_i(x) \equiv b_h(x-a_i) \qquad\qquad i = 1, \ldots, r$$

are a basis for the space of piecewise linear polynomials on $[a, b]$ with breaks at the a_i. (See §2.1 of Schultz [25].) This naturally leads to the idea of finding a better approximation to g by letting $\tilde{g}$ in (3.3) be a higher order interpolant of g. We will now present an algorithm in which $\tilde{g}$ is piecewise cubic.

3.3. Spline Smoothing This may be accomplished in many ways. (For example, see de Boor [4] and Schultz [25].) Here we suggest one method which also has the potential of creating fewer sheets, thus reducing the overall computational cost of the method. We choose a cutoff, $B(x)$, defined by

$$B(x) \equiv \begin{cases} \frac{1}{4}(2-|x|)^3 - (1-|x|)^3, & \text{if } 0 \le |x| \le 1 \\ \frac{1}{4}(2-|x|)^3, & \text{if } 1 \le |x| \le 2 \\ 0, & \text{if } |x| > 2 \end{cases} \tag{3.4}$$

For $b(x) = B(x)$ the b_h are B-splines ([4, 25]). This results in an approximation, $\tilde{u}^k$, which is C^2 in x and piecewise C^3 in x.

Note that with this choice of b the support of b_h is now $4h$ rather than $2h$. Thus, the sheets overlap each other more than with the piecewise linear cutoff defined by (3.2). In particular, each new sheet centered at a_i now influences three grid points rather than just one as is the case for Chorin's smoothing, (3.2). Thus, in the creation algorithm we can no longer simply choose ω_i so that $| u_i + q_i \omega_i | < \omega_{\max}$. Instead, one must now solve the tridiagonal matrix equation

$$\frac{1}{4}\alpha_{i-1} + \alpha_i + \frac{1}{4}\alpha_{i+1} = u_i \qquad\qquad i = 1, \ . \ . \ . \ , r$$

and choose q_i, ω_i so that $| \alpha_i + q_i \omega_i | < \omega_{\max}$. One has to decide what to do at the endpoints, $i = 1$ and $i = r$. Endpoint conditions have been extensively studied in the context of spline interpolation of a function. For example, see de Boor [4]. For the numerical experiments presented in Chapter 6 we used a periodic domain and hence, $a_i = a_{i+r}$.

For the cubic spline cutoff defined in (3.4) the sheet creation algorithm should result in fewer sheets. For example, let $L = 1$ (i.e., a wall of length 1) and consider the periodic problem in which the point $x = b$ is identified with $x = a$. So we have $a_1 = a_{r+1}$, etc. Let $h = 0.2$, $\omega_{\max} = 3^{-1}$, and $u_i = 1.0$, $i = 1, \ . \ . \ . \ , r$. Then for the piecewise linear cutoff $l(x)$ defined in (3.2) we will create 3 sheets at every grid point, each with strength $\omega_i = 3^{-1}$. On the other hand, for the B-spline cutoff defined in (3.4), we would create 2 sheets at every grid point, each with strength $\omega_i = 3^{-1}$.

4. The Error Due to the Random Walk Operator $\widetilde{D}_{\Delta t}$

In this chapter we prove several bounds on the error that results from using the random walk to approximate the exact solution of (2.2a,b). The purpose of these estimates is to examine the relationship between the parameters ν, Δt , $\omega_{\max}$, and h and the error made by one fractional step of the random walk process. We present this analysis to explain how the parameters affect the error at each step. We feel that the analysis below helps to clarify the relationship between the accuracy with which the no-slip boundary condition is satisfied and the error due to the random walk process.

We begin by showing that the random walk algorithm is consistent in the sense that,

$$\| \mathrm{E}\, \widetilde{D}_{\Delta t}\, u^0 - D_{\Delta t}\, u^0 \|_1 = \mathrm{O}((\omega_{\max} + h)\, \sqrt{\nu \Delta t}\,) \,. \tag{4.1}$$

We define u^0, $\widetilde{D}_{\Delta t}\, u^0$ and what we mean by $\mathrm{E}\, \widetilde{D}_{\Delta t}\, u^0$ below. We then derive bounds on the variance of $\widetilde{D}_{\Delta t}\, u^0$ and on the probability distribution of the L^2 error, $\| D_{\Delta t}\, \tilde{u} - \widetilde{D}_{\Delta t}\, \tilde{u} \|_2$. These latter bounds are essentially a generalization of Hald's work in [16]. To establish them we first prove

$$\int_0^\infty var\, \mathrm{H}(\, |\, y_j + \varsigma_j\, | - y\,)\, dy = F\,(y_j)\, \sqrt{2\nu\Delta t} \tag{4.2}$$

for some function F which is bounded between $(2-\sqrt{2})/\sqrt{\pi}$ and $4/\sqrt{\pi}$. (For $y_j = 0$ this is Hald's result.) Then, using the fact that the random walks ς_j taken at a given time step are independent, we use (4.2) to show

$$\| \, var\, (\widetilde{D}_{\Delta t}\, u^0) \|_1 \leq C\, \sqrt{2\nu\Delta t}\, \omega_{\max} \,. \tag{4.3}$$

It will be apparent from the proof that (4.3) exhibits the correct dependence on the parameters ν, Δt and $\omega_{\max}$. Along these same lines we note that Hald has shown

$$\int_0^\infty var\,\Theta(y)\,dy = \frac{(2-\sqrt{2})}{\sqrt{\pi}}\,\sqrt{2\nu\Delta t}\;\omega_{\max}$$

where Θ is the random walk solution after one time step of length Δt to

$$\Theta_t = \nu\,\Theta_{yy} \qquad 0 \le y < \infty,$$

$$\Theta(0,t) = 1 \qquad 0 < t,$$

$$\Theta(y,0) = 0,$$

and where we have written $\omega_{\max}$ instead of N^{-1}. (All of Hald's particles have strength N^{-1}.) This is the second equation in the proof of Theorem 2 in [16]. Thus, the L^1 norm of the variance of Θ is precisely $O(\sqrt{\nu\Delta t}\;\omega_{\max})$. In the case of (4.3) equality generally fails to hold, but the amount by which the right and left hand sides differ does not depend on ν, Δt, and $\omega_{\max}$.

It is important to note that by (4.1) and (4.3), the error in the diffusion step decreases as $\nu \to 0$. Thus, one gets better results from the random walk at small viscosities *for no additional work*. In contrast, for a finite difference method the amount of work to achieve comparable errors at different viscosities increases like $O(\sqrt{\nu}^{-1})$.

4.1. Notation In what follows we will let u^0 be an arbitrary function of the form

$$u^0(x,y) = U(x) + \sum_{j=1}^{N} \omega_j\; b_h(x - x_j)\,\mathrm{H}(y_j - y), \tag{4.4}$$

with $|\omega_j| \le \omega_{\max}$ for all j. We assume the use of piecewise linear smoothing, $b_h(x) \equiv b(x/h)$ with b defined by (3.2). All of the results in this section remain valid (with minor modifications) if B-spline smoothing is used.

We also assume that the y_j in (4.4) have been chosen so that

$$y_i \neq y_j , \qquad i \neq j . \tag{4.5}$$

This gives us a nice representation for the L^1 norm of the vorticity field $\omega^0 = -\partial_y u^0$,

$$\| \omega^0 \|_1 = \int_a^b \int_0^\infty \left| \sum_j \omega_j \; b_h(x - x_j)\, \delta(y_j - y) \right| dx dy = \sum_j |\omega_j| \int_a^b b_h(x - x_j)\, dx \tag{4.6}$$

Note that the sum is over all sheets in the flow. We remark that in the vortex sheet method (without tagging) the probability that $y_i^k = y_j^k$ or $y_i^{k+1/2} = y_j^{k+1/2}$ for some $i \neq j$ is 0. Hence, the assumption (4.5) is reasonable.

We assume that the a_i have been chosen as described in §2.3.2. Define the action of $\widetilde{D}_{\Delta t}$ on u^0 by

$$\widetilde{D}_{\Delta t}\, u^0(x, y) = U(x) + \sum_{j=1}^{N} \omega_j \; b_h(x - x_j)\, \mathrm{H}(\, | y_j + \varsigma_j | - y\,) \tag{4.7}$$

$$+ \sum_{i=1}^{r} \sum_{l=1}^{q_i} \omega_{il} \; b_h(x - a_i)\, \mathrm{H}(\, | \varsigma_{il} | - y\,)$$

where and the ς_j and ς_{il} are independent Gaussian random variables with mean 0 and variance $2\nu\Delta t$ and q_i and ω_{il} are chosen as in Algorithm B. The results below remain true for creation algorithm A or if one solves the BC (2.18) exactly by requiring that

$$\sum_{l=1}^{q_i} \omega_{il} \;=\; - u^0(a_i, 0)$$

hold for each $i = 1, \ldots, r$.

We let $\mathrm{E}\, \widetilde{D}_{\Delta t}\, u^0$ denote the expectation of $\widetilde{D}_{\Delta t}\, u^0$ taken over the random walks ς_j and ς_{il} while

$$var\,(\widetilde{D}_{\Delta t}\,u^0) = \mathrm{E}\,[\,(\widetilde{D}_{\Delta t}\,u^0 - \mathrm{E}\,\widetilde{D}_{\Delta t}\,u^0)^2\,]$$

denotes the variance of $\widetilde{D}_{\Delta t}\,u^0$ with respect to these random walks.

We will obtain bounds in the $L^1(\Omega)$ and $L^2(\Omega)$ norms where Ω is our computational domain $\Omega = [a\,,b\,]\times[0,\infty)$ and for $1 \leq p < \infty$ the $L^p(\Omega)$ norm of the error between two functions is defined by

$$\|f - g\|_p \equiv \left(\int_a^b \int_0^\infty |\,f(x\,,y\,) - g\,(x\,,y\,)\,|^p\,dydx\right)^{\frac{1}{p}}.$$

For a function $f(x\,,y\,)$ defined on Ω we will sometimes need to consider the sup norm of f as a function defined on the wall alone,

$$\|f(\,\cdot\,,0)\|_\infty \equiv \sup_{x\,\in\,[a\,,b\,]} |\,f(x\,,0)\,|\,.$$

Furthermore, if f is piecewise C^1 on $[a\,,b\,]$ and C^1 on the open intervals $(b_{i-1},b_i\,)$ where $a = b_1 \leq \;.\;.\;.\; \leq b_m = b$ then, following Schultz ([25], p. 2), we define

$$\|\partial_x f(\,\cdot\,,0)\|_\infty \equiv \max_i \sup_{b_{i-1}\,\leq\,x\,\leq\,b_i} |\,\partial_x f(x\,,0)\,|\,.$$

The L^2 norm of $f(x\,,0)$ and $\partial_x f(x\,,0)$ are defined similarly.

Recall that we denote the length of the wall by $L = b - a$. In any actual utilization of the vortex sheet method the sheets will be moving downstream parallel to the wall, eventually leaving $[a\,,b\,]$. In particular, at any given time step some sheets will lie partly in and partly out of this interval. Since in this section we are only concerned with movement of the sheets in the direction perpendicular to the wall this will not present a problem. We consider only those parts of sheets which affect the velocity field within the computational domain Ω.

4.2. The Analysis We begin by showing that the exact solution $D_{\Delta t}\, u^0$ is the expected value of our random walk process when the no-slip boundary condition is solved exactly. (In this regard see the definition of $\tilde{u}_{opt}^{k+1}$ in §3.2.)

THEOREM 4.1 Let $u^0(x\,,y\,)$ be given by (4.4) and let $D_{\Delta t}\, u^0$ denote the exact solution of the differential equation (2.2a,b) with initial data u^0. Then

$$D_{\Delta t}\, u^0(x\,,y\,) = \mathrm{E}\,\left[\; U(x\,) + \sum_j \omega_j \;\; b_h(x\,-x_j\,)\,\mathrm{H}(\,|\,y_j + \varsigma_j\;|-y\,) - u^0(x\,,0)\,\mathrm{H}(\,|\,\varsigma\,|\;-y\,)\,\right]$$

where ς and the ς_j are Gaussian distributed random variables with mean 0 and variance $2\nu\Delta t$ and the expected value is over these random variables.

Proof: We begin by obtaining an exact expression for $D_{\Delta t}\, u^0$ in terms of the Green's function for the diffusion equation on $-\infty < y < \infty$. The exact solution to (2.2a,b) on the half plane $y \geq 0$ can be found by extending the initial data anti-symmetrically about $x = 0$,

$$u^0(x\,,y\,) \equiv -\,u^0(x\,,-y\,) \qquad\qquad y < 0,$$

and solving

$$u_t = \nu u_{yy}\,,$$

$$u\,(x\,,y\,,0) = u^0(x\,,y\,),$$

on the entire real line $-\infty < y < \infty$. The solution of this problem is easily obtained via the fundamental solution of the heat equation on $\mathbb{R}$ ([19]),

$$u\,(x\,,y\,,t\,) = \frac{1}{\sqrt{4\pi\nu t}} \int_{-\infty}^{\infty} e^{\frac{-(y-s)^2}{4\nu t}}\; u^0(x\,,s\,)\; ds \tag{4.8}$$

For u^0 defined by (4.4) let $c_j = \omega_j \; b_h(x - x_j)$ where we suppress the dependence on x for notational convenience. Then

$$D_{\Delta t} u^0(x, y) = \int_0^\infty \frac{e^{\frac{-(y-s)^2}{4\nu\Delta t}}}{\sqrt{4\pi\nu\Delta t}} \left(U(x) + \sum_j c_j \; \mathrm{H}(y_j - s)\right) ds$$

$$- \int_{-\infty}^0 \frac{e^{\frac{-(y-s)^2}{4\nu\Delta t}}}{\sqrt{4\pi\nu\Delta t}} \left(U(x) + \sum_j c_j \; \mathrm{H}(y_j + s)\right) ds$$

$$= \int_{-y}^\infty \frac{e^{\frac{-\varsigma^2}{4\nu\Delta t}}}{\sqrt{4\pi\nu\Delta t}} U(x) d\varsigma - \int_{-\infty}^{-y} \frac{e^{\frac{-\varsigma^2}{4\nu\Delta t}}}{\sqrt{4\pi\nu\Delta t}} U(x) d\varsigma$$

$$+ \sum_j c_j \int_{y-y_j}^{y} \frac{e^{\frac{-\varsigma^2}{4\nu\Delta t}}}{\sqrt{4\pi\nu\Delta t}} d\varsigma + \sum_j c_j \int_{-y}^{-y-y_j} \frac{e^{\frac{-\varsigma^2}{4\nu\Delta t}}}{\sqrt{4\pi\nu\Delta t}} d\varsigma$$

$$= \int_{-\infty}^\infty \frac{e^{\frac{-\varsigma^2}{4\nu\Delta t}}}{\sqrt{4\pi\nu\Delta t}} U(x) d\varsigma - 2 \int_{-\infty}^{-y} \frac{e^{\frac{-\varsigma^2}{4\nu\Delta t}}}{\sqrt{4\pi\nu\Delta t}} U(x) d\varsigma$$

$$+ \sum_j c_j \int_{y-y_j}^{\infty} \frac{e^{\frac{-\varsigma^2}{4\nu\Delta t}}}{\sqrt{4\pi\nu\Delta t}} d\varsigma + \sum_j c_j \int_{-\infty}^{-y-y_j} \frac{e^{\frac{-\varsigma^2}{4\nu\Delta t}}}{\sqrt{4\pi\nu\Delta t}} d\varsigma$$

$$- \sum_j c_j \int_{y}^{\infty} \frac{e^{\frac{-\varsigma^2}{4\nu\Delta t}}}{\sqrt{4\pi\nu\Delta t}} d\varsigma - \sum_j c_j \int_{-\infty}^{-y} \frac{e^{\frac{-\varsigma^2}{4\nu\Delta t}}}{\sqrt{4\pi\nu\Delta t}} d\varsigma$$

$$= U(x) + \sum_j c_j \int_{-y_j}^{\infty} \frac{e^{\frac{-\varsigma^2}{4\nu\Delta t}}}{\sqrt{4\pi\nu\Delta t}} \mathrm{H}(y_j + \varsigma - y) d\varsigma + \sum_j c_j \int_{-\infty}^{-y_j} \frac{e^{\frac{-\varsigma^2}{4\nu\Delta t}}}{\sqrt{4\pi\nu\Delta t}} \mathrm{H}(-y_j - \varsigma - y) d\varsigma$$

$$- \left(U(x) + \sum_j c_j\right) \int_{-\infty}^{\infty} \frac{e^{\frac{-\varsigma^2}{4\nu\Delta t}}}{\sqrt{4\pi\nu\Delta t}} \mathrm{H}(|\varsigma| - y) d\varsigma$$

$$= U(x) + \sum_j c_j \int_{-\infty}^{\infty} \frac{e^{\frac{-\varsigma^2}{4\nu\Delta t}}}{\sqrt{4\pi\nu\Delta t}} \mathrm{H}(\,|\,y_j + \varsigma\,| - y\,)\,d\varsigma - u^0(x,0) \int_{-\infty}^{\infty} \frac{e^{\frac{-\varsigma^2}{4\nu\Delta t}}}{\sqrt{4\pi\nu\Delta t}} \mathrm{H}(\,|\,\varsigma\,| - y\,)\,d\varsigma$$

$$= U(x) + \sum_j c_j \,\mathrm{E}\,\mathrm{H}(\,|\,y_j + \varsigma\,| - y\,) - u^0(x,0)\,\mathrm{E}\,\mathrm{H}(\,|\,\varsigma\,| - y\,)\,.$$

Thus, the amount by which the expected value of $\widetilde{D}_{\Delta t}\, u^0$ differs from the exact solution, $D_{\Delta t}\, u^0$, depends on how well one approximates $u^0(x,0)$ by creating new sheets at the wall. We will now show that in the L^1 norm this difference is $\mathrm{O}((h + \omega_{\max})\sqrt{\nu\Delta t})$. This fact holds for either of the particle creation algorithms described in §2.3.2 as well as solving the BC (2.18) exactly.

THEOREM 4.2: Let u^0, $\widetilde{D}_{\Delta t}\, u^0$ be defined by (4.4) and (4.7) respectively. Then

$$\|\,\mathrm{E}\,\widetilde{D}_{\Delta t}\, u^0 - D_{\Delta t}\, u^0\,\|_1 \le \frac{L}{\sqrt{\pi}}\,[\,\frac{1}{2}\,\|\,\partial_x\, u^0(\,\cdot\,,0)\,\|_\infty\, h + \omega_{\max}\,]\,\sqrt{4\nu\Delta t}\,. \tag{4.9}$$

Proof: Let $u_i^l = -\sum_{l=1}^{q_i} \omega_{il}$. By Theorem 4.1 we have

$$\mathrm{E}\,\widetilde{D}_{\Delta t}\, u^0(x,y) - D_{\Delta t}\, u^0(x,y) = \mathrm{E}\,[\,\sum_{i=1}^{r}\sum_{l=1}^{q_i} \omega_{il}\; b_h(x - a_i)\,\mathrm{H}(\,|\,\varsigma_{il}\,| - y\,)\,]$$

$$+ \mathrm{E}\,[\,u^0(x,0)\,\mathrm{H}(\,|\,\varsigma\,| - y\,)\,] \tag{4.10}$$

$$= -\,[\,\sum_{i=1}^{r} u_i^l\; b_h(x - a_i) - u^0(x,0)\,]\,\mathrm{E}\,\mathrm{H}(\,|\,\varsigma\,| - y\,)\,.$$

since ς and the ς_{il} are identically distributed. Thus,

$$\|\,\mathrm{E}\,\widetilde{D}_{\Delta t}\, u^0 - D_{\Delta t}\, u^0\,\|_1 = \int_a^b |\,\sum_{i=1}^{r} u_i^l\, b_h(x - a_i) - u^0(x,0)\,|\;dx \int_0^{\infty} \mathrm{E}\,\mathrm{H}(\,|\,\varsigma\,| - y\,)\,dy\,.$$

We can write

$$\mathrm{E}\,\mathrm{H}(\,|\,\varsigma\,|-y\,)=\int_{-\infty}^{\infty}\mathrm{H}(\,|\,\varsigma\,|-y\,)\,\frac{e^{\frac{-\varsigma^2}{4\nu\Delta t}}}{\sqrt{4\pi\nu\Delta t}}\,d\varsigma=\int_{y/\sqrt{2\nu\Delta t}}^{\infty}\frac{2e^{-\varsigma^2/2}}{\sqrt{2\pi}}\,d\varsigma \tag{4.11}$$

whereby

$$\int_0^{\infty}\mathrm{E}\,\mathrm{H}(\,|\,\varsigma\,|-y\,)\,dy=\int_0^{\infty}\int_{y/\sqrt{2\nu\Delta t}}^{\infty}\frac{2e^{-\varsigma^2/2}}{\sqrt{2\pi}}\,d\varsigma dy=\frac{\sqrt{4\nu\Delta t}}{\sqrt{\pi}}\int_0^{\infty}\int_y^{\infty}e^{-\varsigma^2/2}\,d\varsigma dy=\frac{\sqrt{4\nu\Delta t}}{\sqrt{\pi}}\,.$$

The last equality follows from integration by parts with respect to y. Next, let $u_i = u^0(a_i,0)$ and write

$$\int_a^b\Big|\sum_{i=1}^{r}u_i^{\prime}\,b_h(x-a_i)-u^0(x,0)\Big|\,dx\le\int_a^b\Big|\sum_{i=1}^{r}u_i^{\prime}\,b_h(x-a_i)-\sum_{i=1}^{r}u_i\,b_h(x-a_i)\Big|\,dx$$

$$+\int_a^b\Big|\sum_{i=1}^{r}u_i\,b_h(x-a_i)-u^0(x,0)\Big|\,dx$$

By definition of the $u_i^{\prime}$ and (2.20) we have

$$|\,u_i^{\prime}-u_i\,|\;=\;|\,q_i\,\omega_i+u_i\,|\;<\;\omega_{\max}\,. \tag{4.12}$$

Thus, since $rh = L$,

$$\int_a^b\Big|\sum_{i=1}^{r}u_i^{\prime}\,b_h(x-a_i)-\sum_{i=1}^{r}u_i\,b_h(x-a_i)\Big|\,dx<\omega_{\max}\sum_{i=1}^{r}\int_a^b b_h(x-a_i)\,dx\le L\;\omega_{\max}$$

where we have used (3.2) to evaluate the integral of b_h exactly. Now note that $\sum u_i\,b_h(x-a_i)$ is the piecewise linear interpolant of $u^0(x,0)$ with breaks at the a_i. Therefore, exercise 2.3 of Schultz ([25]) implies

$$\int_a^b \left| \sum_{i=1}^{r} u_i\, b_h(x-a_i) - u^0(\cdot,0) \right| dx \le \frac{1}{2} L\ h\ \|\partial_x u^0(\cdot,0)\|_\infty .$$

The theorem follows immediately.

During the course of estimating the probability distribution of the error in the L^2 norm (Theorem 4.7) we will need the following bound.

THEOREM 4.3: For u^0 and $\widetilde{D}_{\Delta t} u^0$, as in Theorem 4.2 we have

$$\|\mathrm{E}\,\widetilde{D}_{\Delta t} u^0 - D_{\Delta t} u^0\|_2 \le \left(\frac{2(\sqrt{2}-1)}{\sqrt{\pi}}\right)^{\frac{1}{2}} \left(\sqrt{L}\ \omega_{\max} + \pi^{-1}\ \|\partial_x u^0(\cdot,0)\|_2\, h\right)(2\nu\Delta t)^{\frac{1}{4}} .$$

Proof: From (4.10) we find

$$\|\mathrm{E}\,\widetilde{D}_{\Delta t} u^0 - D_{\Delta t} u^0\|_2 = \left(\int_a^b \left(\sum_{i=1}^{r} u_i^l\, b_h(x-a_i) - u^0(x,0)\right)^2 dx\right)^{\frac{1}{2}} \left(\int_0^\infty (\mathrm{E}\,\mathrm{H}(|\varsigma|-y))^2 dx\right)^{\frac{1}{2}}. \qquad (4.13)$$

The right hand side of (4.13) is the product of two one dimensional norms. The first of these is the L^2 norm of a function of x defined on the interval $[a,b]$. Letting $u_i = u^0(a_i,0)$ we have

$$\left\|\sum_{i=1}^{r} u_i^l\, b_h(\cdot - a_i) - u^0(\cdot,0)\right\|_2 \le \left\|\sum_{i=1}^{r} u_i^l\, b_h(\cdot - a_i) - \sum_{i=1}^{r} u_i\, b_h(\cdot - a_i)\right\|_2$$

$$+ \left\|\sum_{i=1}^{r} u_i\, b_h(\cdot - a_i) - u(\cdot,0)\right\|_2$$

We can evaluate the first term on the right by using (4.12) and the fact that $\sum b_h(x-a_i) \le 1$ for all x (since $a_i - a_{i-1} = h$),

$$\left\|\sum_{i=1}^{r} u_i^l\, b_h(\cdot - a_i) - \sum_{i=1}^{r} u_i\, b_h(\cdot - a_i)\right\|_2 < \omega_{\max}\sqrt{L} .$$

To evaluate the second expression we use Theorem 2.4 of Schultz ([25]) to bound the L^2 norm of the difference between $u^0(x,0)$ and the piecewise linear interpolant $\sum u_i\, b_h(x-a_i)$,

$$\| \sum_{i=1}^{r} u_i\, b_h(\cdot - a_i) - u^0(\cdot,0) \|_2 \leq \pi^{-1} \, \| \partial_x u^0(\cdot,0) \|_2 \, h \ .$$

The other one dimensional norm on the right hand side of (4.13) may be evaluated by using (4.11) and Lemma 1 of Hald ([16]) with $a = b = 2\nu\Delta t$,

$$\Big(\int_0^\infty (\mathrm{E}\,\mathrm{H}(|\varsigma| - y))^2 dy\Big)^{\frac{1}{2}} = \Big(\int_0^\infty \int_{y/\sqrt{2\nu\Delta t}}^\infty \frac{2e^{-\varsigma^2/2}}{\sqrt{2\pi}} d\varsigma \int_{y/\sqrt{2\nu\Delta t}}^\infty \frac{2e^{-\varsigma^2/2}}{\sqrt{2\pi}} d\varsigma dy\Big)^{\frac{1}{2}}$$

$$= \Big(\frac{2(\sqrt{2}-1)}{\sqrt{\pi}}\Big)^{\frac{1}{2}} (2\nu\Delta t)^{\frac{1}{4}} \ .$$

We would like a bound on the L^1 norm of the variance of $\widetilde{D}_{\Delta t} u^0$. We begin with two preliminary lemmas, the first of which is essentially an extension Hald's Lemma 1 ([16]).

LEMMA 4.4: For any $y_j \geq 0$ we have

$$\int_0^\infty \int_y^\infty \frac{2e^{-(\varsigma - y_j)^2/2}}{\sqrt{2\pi}} d\varsigma \int_0^y \frac{2e^{-(\varsigma - y_j)^2/2}}{\sqrt{2\pi}} d\varsigma dy = F(y_j) \tag{4.14}$$

where

$$F(y) = \frac{2}{\pi}\Big(\sqrt{2} - e^{-\frac{y^2}{2}}\Big)\Big(\frac{\sqrt{\pi}}{\sqrt{2}} + \int_0^y e^{-\varsigma^2/2} d\varsigma\Big) + \frac{2\sqrt{2}}{\pi} \int_y^{\sqrt{2}y} e^{-\varsigma^2/2} d\varsigma \ . \tag{4.15}$$

Furthermore, $F(0) = (2-\sqrt{2})/\sqrt{\pi}$, $F'(y) \geq 0$ for all y, and $F(\infty) = 4/\sqrt{\pi}$ implying

$$\frac{(2-\sqrt{2})}{\sqrt{\pi}} \leq F(y) \leq \frac{4}{\sqrt{\pi}} \tag{4.16}$$

for all $y \in [0,\infty)$.

Proof: Our proof closely follows Hald's. Set

$$f(y) = \int_0^y e^{-(\varsigma - y_j)^2/2} d\varsigma .$$

By interchanging the order of integration and then integrating the inside integral by parts we obtain

$$F(y_j) = \frac{2}{\pi} \int_0^\infty e^{-(\varsigma - y_j)^2/2} \int_0^\varsigma f(y)\, dy\, d\varsigma$$

$$= \frac{2}{\pi} \int_0^\infty e^{-(\varsigma - y_j)^2/2} [\, \varsigma f(\varsigma) + e^{-(\varsigma - y_j)^2/2} - e^{-y_j{}^2/2} - y_j\ f(\varsigma)\,] d\varsigma$$

$$= \frac{2}{\pi} \int_0^\infty e^{-(\varsigma - y_j)^2/2} (\varsigma - y_j)\, f(\varsigma) + e^{-(\varsigma - y_j)^2/2} e^{-(\varsigma - y_j)^2/2} - e^{-y_j{}^2/2}\ e^{-(\varsigma - y_j)^2/2} d\varsigma .$$

Now integrate the first summand in this last expression by parts to get

$$F(y_j) = \frac{2}{\pi} [\, 2 \int_0^\infty e^{-(\varsigma - y_j)^2} d\varsigma - e^{-y_j{}^2/2} \int_0^\infty e^{-(\varsigma - y_j)^2/2} d\varsigma\,]$$

$$= \frac{2}{\pi} [2 \int_{-y_j}^\infty e^{-\varsigma^2} d\varsigma - e^{-y_j{}^2/2} \int_{-y_j}^\infty e^{-\varsigma^2/2} d\varsigma]$$

$$= \frac{2}{\pi} [(\sqrt{2} - e^{-y_j{}^2/2}) \int_0^\infty e^{-\varsigma^2/2} d\varsigma + \sqrt{2} \int_{-\sqrt{2}y_j}^0 e^{-\varsigma^2/2} d\varsigma - e^{-y_j{}^2/2} \int_{-y_j}^0 e^{-\varsigma^2/2} d\varsigma]$$

$$= \frac{2}{\pi} [(\sqrt{2} - e^{-y_j{}^2/2}) (\frac{\sqrt{\pi}}{\sqrt{2}} + \int_0^{y_j} e^{-\varsigma^2/2} d\varsigma) + \sqrt{2} \int_{y_j}^{\sqrt{2}y_j} e^{-\varsigma^2/2} d\varsigma]$$

This proves (4.14). The claims regarding $F(0)$, $F'(y)$ and $F(\infty)$ are easily verifiable.

We obtain bounds on the variance of $\widetilde{D}_{\Delta t} u^0$ using the following bound on the L^1 norm of the variance of the independent summands, $\mathrm{H}(\,|\,y_j+\varsigma_j\,|-y\,)$. Hald proved this lemma in [16] for the case when $y_j=0$.

LEMMA 4.5: Let $y_j \geq 0$, let $F(y_j)$ be defined by (4.15), and let ς be a Gaussian random variable with mean 0 and variance $2\nu\Delta t$. Then

$$\int_0^\infty var\,\mathrm{H}(\,|\,y_j+\varsigma\,|-y\,)dy \leq F(y_j/\sqrt{2\nu\Delta t})\sqrt{2\nu\Delta t}\,.$$

Proof: First note that

$$\mathrm{E}\,\mathrm{H}(\,|\,y_j+\varsigma\,|-y\,) = \int_{-\infty}^{\infty} \mathrm{H}(\,|\,y_j+\varsigma\,|-y\,)\,\frac{e^{\frac{-\varsigma^2}{4\nu\Delta t}}}{\sqrt{4\pi\nu\Delta t}}\,d\varsigma = P(\,|\,y_j+\varsigma\,|\geq y\,)\,.$$

Hence, since $\mathrm{H}(y)^2=\mathrm{H}(y)$ and $1-P(a\geq b)=P(a<b)$, we have

$$var\,\mathrm{H}(\,|\,y_j+\varsigma\,|-y\,) = P(\,|\,y_j+\varsigma\,|\geq y\,)\;P(\,|\,y_j+\varsigma\,|<y\,)\,.$$

Furthermore,

$$P(\,|\,y_j+\varsigma\,|\geq y\,) = \int_{-\infty}^{\infty} \mathrm{H}(\,|\,y_j+\varsigma\,|-y\,)\,\frac{e^{\frac{-\varsigma^2}{4\nu\Delta t}}}{\sqrt{4\pi\nu\Delta t}}\,d\varsigma$$

$$= \int_y^\infty \frac{e^{\frac{-(\varsigma-y_j)^2}{4\nu\Delta t}}}{\sqrt{4\pi\nu\Delta t}}\,d\varsigma + \int_{-\infty}^{-y} \frac{e^{\frac{-(\varsigma-y_j)^2}{4\nu\Delta t}}}{\sqrt{4\pi\nu\Delta t}}\,d\varsigma$$

$$\leq \int_y^\infty \frac{2e^{\frac{-(\varsigma-y_j)^2}{4\nu\Delta t}}}{\sqrt{4\pi\nu\Delta t}}\,d\varsigma$$

since the Gaussian curve is centered at $\varsigma = y_j$. Similarly, we have

$$P(\,|\,y_j+\varsigma\,|\;<\;y\;) = \int_{-\infty}^{\infty} \mathrm{H}(y-|\,y_j+\varsigma\,|\,)\,\frac{e^{\frac{-\varsigma^2}{4\nu\Delta t}}}{\sqrt{4\pi\nu\Delta t}}\,d\varsigma$$

$$= \int_0^y \frac{e^{\frac{-(\varsigma-y_j)^2}{4\nu\Delta t}}}{\sqrt{4\pi\nu\Delta t}}\,d\varsigma + \int_{-y}^0 \frac{e^{\frac{-(\varsigma-y_j)^2}{4\nu\Delta t}}}{\sqrt{4\pi\nu\Delta t}}\,d\varsigma$$

$$\leq \int_0^y \frac{2e^{\frac{-(\varsigma-y_j)^2}{4\nu\Delta t}}}{\sqrt{4\pi\nu\Delta t}}\,d\varsigma\,.$$

Now let $z_j = y_j/\sqrt{2\nu\Delta t}$. Then we have

$$\int_0^\infty var\,\mathrm{H}(\,|\,y_j+\varsigma\,|\;-y\,)dy = \int_0^\infty P(\,|\,y_j+\varsigma\,|\;\geq y\,)\,P(\,|\,y_j+\varsigma\,|\;<\;y\,)dy$$

$$\leq \int_0^\infty \int_y^\infty \frac{2e^{\frac{-(\varsigma-y_j)^2}{4\nu\Delta t}}}{\sqrt{4\pi\nu\Delta t}}\,d\varsigma \int_0^y \frac{2e^{\frac{-(\varsigma-y_j)^2}{4\nu\Delta t}}}{\sqrt{4\pi\nu\Delta t}}\,d\varsigma dy$$

$$= \int_0^\infty \int_{y/\sqrt{2\nu\Delta t}}^\infty \frac{2e^{-(\varsigma-z_j)^2/2}}{\sqrt{2\pi}}\,d\varsigma \int_0^{y/\sqrt{2\nu\Delta t}} \frac{2e^{-(\varsigma-z_j)^2/2}}{\sqrt{2\pi}}\,d\varsigma dy$$

$$= \sqrt{2\nu\Delta t}\;F(z_j)\,.$$

A bound on the L^1 norm of the variance of $\widetilde{D}_{\Delta t}\,u^0$ now follows easily from the independence of the random walks, ς_j and ς_{il}.

THEOREM 4.6: Let u^0 be given by (4.4) and $\widetilde{D}_{\Delta t}\,u^0$ by (4.7). Then

$$\|\;var\,(\widetilde{D}_{\Delta t}\,u^0)\;\|_1 \leq\; C_v\;\sqrt{2\nu\Delta t}\;\omega_{\max} \tag{4.17}$$

where

$$C_v = \frac{4}{\sqrt{\pi}} \left\{ \| \omega^0 \|_1 + \frac{2}{3} L \ \| u^0(\cdot, 0) \|_\infty \right\} .$$

Proof: Since the ς_j and ς_{il} are independent, identically distributed random variables we have

$$\| var(\widetilde{D}_{\Delta t} u^0) \|_1 = \int_a^b \int_0^\infty \sum_j \omega_j^2 \, b_h^2(x - x_j) \, var \, \mathrm{H}(\, | \, y_j + \varsigma_j \, | - y \,) dy dx$$

$$+ \int_a^b \int_0^\infty \sum_{i=1}^r \sum_{l=1}^{q_i} \omega_{il}^2 \, b_h^2(x - a_i) \, var \, \mathrm{H}(\, | \, \varsigma_{il} \, | - y \,) dy dx \tag{4.18}$$

$$= \sum_j \omega_j^2 \int_a^b b_h^2(x - x_j) dx \int_0^\infty var \, \mathrm{H}(\, | \, y_j + \varsigma | - y \,) dy$$

$$+ \sum_{i=1}^r \sum_{l=1}^{q_i} \omega_{il}^2 \int_a^b b_h^2(x - a_i) dx \int_0^\infty var \, \mathrm{H}(\, | \, \varsigma | - y \,) dy$$

Since $0 \leq b_h(x) \leq 1$ for all x we have

$$\int_a^b b_h^2(x - x_j) dx \leq \int_a^b b_h(x - x_j) dx$$

and hence, by (4.6)

$$\sum_j \omega_j^2 \int_a^b b_h^2(x - x_j) dx \leq \omega_{\max} \sum_j | \, \omega_j \, | \int_a^b b_h(x - x_j) dx = \omega_{\max} \, \| \omega^0 \|_1 .$$

Furthermore, for the piecewise linear b_h we have

$$\int_a^b b_h^2(x - a_i) dx \ \leq \ h \int_{-1}^1 l^2(x) dx \ = \ \frac{2}{3} h \tag{4.19}$$

where l is defined by (3.2). By definition of the q_i and the ω_i, we find

$$\sum_{l=1}^{q_i} \omega_{il}^2 = \omega_{\max} \sum_{l=1}^{q_i} \mid \omega_{il} \mid \leq \omega_{\max} \mid u^0(a_i, 0) \mid \leq \omega_{\max} \| u^0(\cdot, 0) \|_\infty . \tag{4.20}$$

Thus, by Lemma 4.5 and the fact that $rh = L$ we have

$$\| var(\widetilde{D}_{\Delta t} u^0) \|_1 \leq F(\infty) \left\{ \| \omega^0 \|_1 + \frac{2}{3} L \ \| u^0(\cdot, 0) \|_\infty \right\} \sqrt{2\nu\Delta t}\ \omega_{\max} . \tag{4.21}$$

The inequality in (4.17) now follows from (4.16).

The inequality in (4.17) give us a relationship between the variance of $\widetilde{D}_{\Delta t} u^0$ and the parameters ν, Δt, and $\omega_{\max}$. In particular we see that, in the L^1 norm, the variance of $\widetilde{D}_{\Delta t} u^0$ decreases like $\sqrt{\nu}$. In other words the statistical fluctuations in the actual realization of our random walk, $\widetilde{D}_{\Delta t} u^0$, diminish with diminishing ν. We note in passing that a close inspection of the proof will reveal that the bound in (4.17) exhibits the correct dependence on ν, Δt, and $\omega_{\max}$.

Note too that this proof relies on the independence of the random walks. When sheet tagging is used this independence is in general lost since sheets with the same tag may overlap. This loss of independence results in a term of the form

$$\int_a^b \int_0^\infty \sum_{j \neq l} \omega_j \omega_l \ b_h(x - x_j)\, b_h(x - x_l)\, \mathrm{E}\left[\mathrm{H}(\mid y_j + \varsigma_j \mid - y)\, \mathrm{H}(\mid y_l + \varsigma_l \mid - y) \right] dy dx,$$

$$- \int_a^b \int_0^\infty \sum_{j \neq l} \omega_j \omega_l \ b_h(x - x_j)\, b_h(x - x_l)\, \mathrm{E}\, \mathrm{H}(\mid y_j + \varsigma_j \mid - y)\, \mathrm{E}\, \mathrm{H}(\mid y_l + \varsigma_l \mid - y) dy dx,$$

being added to the right hand side of (4.18) where the sum is over all sheets, new and old. It is hard to see how this will lead to a smaller variance.

Finally, we derive a bound on the probability distribution of the error $\widetilde{D}_{\Delta t} u^0 - D_{\Delta t} u^0$ in the L^2 norm. Our proof is based on ideas found in the proof of Hald 's Theorem 2 ([16]).

THEOREM 4.7: Assume that $h^2 \leq \omega_{\max} \leq 1$ and let u^0 and $\widetilde{D}_{\Delta t} u^0$ be as in Theorem 4.2. Then for all $\gamma > 0$ we have

$$P\left(\| \widetilde{D}_{\Delta t} u^0 - D_{\Delta t} u^0 \|_2 \geq \gamma \sqrt{\omega_{\max}} \right) \leq C_D \sqrt{2\nu\Delta t}\ \gamma^{-2} \tag{4.22}$$

where C_D is defined by

$$C_D = C_v + \frac{2(\sqrt{2}-1)}{\sqrt{\pi}} \left(\sqrt{L} + \pi^{-1} \| \partial_x u^0(\cdot,0) \|_\infty \right)^2 .$$

Remark: As described in Chapter 8 of [21] the bound in (4.22) immediately yields a bound on the expected value of the error,

$$\mathrm{E}\ \| \widetilde{D}_{\Delta t} u^0 - D_{\Delta t} u^0 \|_2 \leq (1 + 2C_D)\,(2\nu\Delta t)^{\frac{1}{4}} \sqrt{\omega_{\max}} .$$

Proof: From Chebychev's inequality (Feller [12], p. 151) we find

$$P\left(\| \widetilde{D}_{\Delta t} u^0 - D_{\Delta t} u^0 \|_2 \geq \gamma \sqrt{\omega_{\max}} \right) \leq \frac{\mathrm{E}\left[\| \widetilde{D}_{\Delta t} u^0 - D_{\Delta t} u^0 \|_2^2 \right]}{\omega_{\max}\, \gamma^2} .$$

We have

$$\begin{aligned}
\mathrm{E}\,(\widetilde{D}_{\Delta t} u^0 - D_{\Delta t} u^0)^2 &= \mathrm{E}\,(\widetilde{D}_{\Delta t} u^0 - \mathrm{E}\,\widetilde{D}_{\Delta t} u^0)^2 \\
&\quad + 2\,\mathrm{E}\left[(\widetilde{D}_{\Delta t} u^0 - \mathrm{E}\,\widetilde{D}_{\Delta t} u^0)(\mathrm{E}\,\widetilde{D}_{\Delta t} u^0 - D_{\Delta t} u^0) \right] + \mathrm{E}\,(\mathrm{E}\,\widetilde{D}_{\Delta t} u^0 - D_{\Delta t} u^0)^2 \\
&= var\,(\widetilde{D}_{\Delta t} u^0) + (\mathrm{E}\,\widetilde{D}_{\Delta t} u^0 - D_{\Delta t} u^0)^2
\end{aligned}$$

and so, by Fubini's theorem,

$$\mathrm{E}\left[\| \widetilde{D}_{\Delta t} u^0 - D_{\Delta t} u^0 \|_2^2 \right] = \| var\, \widetilde{D}_{\Delta t} \|_1 + \| \mathrm{E}\,\widetilde{D}_{\Delta t} u^0 - D_{\Delta t} u^0 \|_2^2 .$$

The bound in (4.22) now follows from Theorems 4.3, 4.6 and our assumption that $h^2 \leq \omega_{\max}$.

4.3. Remarks Theorem 4.2 states that the random walk process is consistent. The term in (4.9) which is $O(\omega_{\max})$ is due to how much we failed to satisfy the no slip boundary condition at the grid points, a_i, $i = 1, \ldots, r$. The $O(h)$ term is the error due to using a piecewise linear interpolation to the tangential velocity at the wall. If we use a higher order interpolation the order of this error increases. For example, with B-spline smoothing it is $O(h^2)$. It will be apparent from the numerical results presented in §6.5 that such an increase in accuracy appears to result in little improvement in the overall accuracy of the method. However it may increase the rate at which the method converges as a function of h.

Based on the experimental evidence in Chapter 6 we believe that large errors in the vortex sheet method manifest themselves in the production of large quantities of unnecessary sheets. Note that in all of the bounds above the constants depend on u^0. In particular, they depend on the L^1 norm of the vorticity, ω^0, and on the size of the tangential velocity at the wall, $u^0(x, 0)$. By (4.6), the vorticity is connected to h and the number of sheets, N, in the following way

$$\|\omega^0\|_1 = \sum_j |\omega_j| \int_a^b b_h(x - x_j)\,dx \approx h\ N\ \omega_{\max}. \tag{4.23}$$

Furthermore, equality fails to hold only because some sheets do not lie entirely in $a \leq x \leq b$. Thus, the L^1 norm of the vorticity grows when the number of sheets in the flow grows faster than to the rate at which h is decreased. We suspect that this is a major source of error in the vortex sheet method. In §6.6 we investigate numerically the increase in vorticity as a function of h, Δt and $\omega_{\max}$ and find that decreasing $\omega_{\max}$ while leaving h fixed results in no appreciable increase in the amount of vorticity in the flow. However, if we fix $\omega_{\max}$ and decrease h the L^1 norm of the vorticity generally grows. The bounds here tell us that this could result in larger errors and the numerical evidence in §6.6 appears to confirm this.

5. The CFL Condition and Dependence of the Method on ν

In this chapter we examine the so called 'CFL condition', $U\Delta t \leq h$, where U is the maximum size of the free stream velocity, $U \equiv \max_x U(x)$. We also discuss the behavior of the vortex sheet method in the limit of vanishing viscosity. In this regard we show that vortex sheet solutions scale like $\sqrt{\nu}$ in the y direction and that, as a consequence , for $1 \leq p < \infty$ the L^p norm of the error in approximating any similarity solution of the Prandtl equations goes to 0 like $\nu^{1/2p}$. On the basis of this example as well as the results in Chapter 4 we argue that vortex sheet method exhibits benign if not favorable dependence on the viscosity.

5.1. The CFL Condition The most well known and perhaps the only universally acknowledged condition on the parameters in the vortex sheet method is

$$U\Delta t \leq O(h) . \tag{5.1}$$

This requirement was proposed by Chorin in [9]. The justification usually given for (5.1) is that one wants to ensure that the distance a sheet travels in one time step parallel to the wall is less than or equal to one sheet length length. Thus, sheets created at the i th grid point are required to influence the $i+1$st grid point before moving on downstream.

We propose another, similar constraint:

$$\Delta t \leq h . \tag{5.2}$$

Consider sheets created at the first grid point, $a_1 = \frac{h}{2}$, during the k th time step. At the next time step, since the velocity is 0 at the wall, the only movement imparted to these sheets will be due to the random walk ς_j in (2.21b). We seek a condition to ensure that these sheets remain in the boundary layer after this random walk.

For Blasius flow the boundary layer thickness at a_1, denoted by δ_{a_1}, is given by

$$\delta_{a_1} = 5\sqrt{\nu a_1} = 5\sqrt{\nu h/2}\,.$$

(Schlichting [24], p. 140). The ς_j are drawn from a Gaussian distribution with mean 0 and standard deviation $\sigma = \sqrt{2\nu\Delta t}$. Thus, if (5.2) holds, then

$$\frac{5}{2}\sigma \leq \delta_{a_1}\,.$$

This implies that, on the average, better than 98% of the sheets created at a_1 will remain in the boundary layer after taking one time step. Since for the Blasius flow the boundary layer increases as x increases this will hold true for the sheets created at the other grid points as well. Similar conditions may be found for other flows, all that is required is an estimate of the boundary layer thickness. We note that for $U = O(1)$ the conditions (5.1) and (5.2) are essentially equivalent. In all computer experiments reported on in this paper Δt and h satisfy (5.2).

5.2. The Dependence of the Vortex Sheet Method on the Viscosity The vortex sheet method scales like $\sqrt{\nu}$. To see this, fix the the parameters Δt, h, $\omega_{\max}$, and the wall length, $b - a = rh$. Let ν_1, $\nu_2 > 0$ and define $\rho = \sqrt{\nu_2/\nu_1}$. Let $(\tilde{u}_1, \tilde{v}_1)$ and $(\tilde{u}_2, \tilde{v}_2)$ denote the vortex sheet solution at some arbitrary time, $t = k\,\Delta t$, with viscosities ν_1 and ν_2 respectively where we use the *same random number sequence* to compute each solution and where the positions of sheets at time 0 are identical modulo the scaling

$$(x_1, y_1) \rightarrow (x_2, y_2) = (x_1, \rho y_1)\,. \tag{5.3}$$

Then,

$$\tilde{u}_2(x,y) = \tilde{u}_1(x,\rho^{-1}y) \ , \qquad \tilde{v}_2(x,y) = \rho^{-1}\tilde{v}_1(x,\rho^{-1}y) \ . \tag{5.4}$$

This follows from induction on the time step and the fact that if ς is a Gaussian distributed random variable with mean 0 and variance $2\nu_1\Delta t$, then $\rho\varsigma$ is a Gaussian random number with mean 0 and variance $2\nu_2\Delta t$.

This invariance of the vortex sheet method under the scaling (5.3) has two important consequences. First, one can not use the vortex sheet method *by itself* to model flows that become unstable at small ν. Instead, one must employ a hybrid method as in Chorin [11]. Second, for $1 \leq p < \infty$ the L^p norm of the error in approximating Blasius flow (see §6.1) scales like $(\sqrt{\nu})^{\frac{1}{p}}$. To see this, let u_1 (*resp.* u_2) denote the exact solution to Blasius flow with viscosity ν_1 (*resp.* ν_2). Then using the change of variables (5.3) and the identity in (5.4) we find

$$\| u_2 - \tilde{u}_2 \|_p = \left(\int_a^b \int_0^\infty | u_2(x,y) - \tilde{u}_2(x,y) |^p \, dy dx \right)^{\frac{1}{p}}$$

$$= \rho^{\frac{1}{p}} \left(\int_a^b \int_0^\infty | u_1(x,y) - \tilde{u}_1(x,y) |^p \, dy dx \right)^{\frac{1}{p}}$$

Thus, if we fix $\nu_1 = 1$ and let $\nu_2 \to 0$ we have

$$\| u_2 - \tilde{u}_2 \|_p = \nu_2^{\frac{1}{2p}} \| u_1 - \tilde{u}_1 \|_p \to 0 \ .$$

Of course this argument works equally well for any similarity solution of the Prandtl equations which has similarity scaling

$$\eta = y / \sqrt{\nu x} \ .$$

In particular, this argument applies to the Falkner-Skan solutions (Schlichting [24], Chapter IX) and hence the error will scale with ν for any flow which is converges to these solutions. (e.g.,

Serrin [26]).

In general, we believe that the vortex sheet method exhibits either a 'favorable' dependence on ν or no dependence at all. (The latter is probably the case for errors in the sup norm.) For example, the results in Chapter 4 show how the error due to the random walk improves with decreasing ν. This independence of ν is what makes the vortex sheet method competitive.

6. Numerical Results

6.1. The Test Problem We model 2-D flow past a flat plate with a constant free stream velocity, $U(x) \equiv const$. This is known as Blasius flow ([24, 31]). For simplicity we take the constant equal to 1, so $U(x) \equiv 1$. This is a stationary flow which has a well known similarity solution,

$$u(x,y) = f'(\eta) \tag{6.1}$$

where

$$\eta = y \ / \ \sqrt{\nu x} \tag{6.2}$$

and f satisfies the ODE

$$ff'' + 2f''' = 0 \tag{6.3a}$$

$$f(0) = 0, \quad f'(0) = 0, \quad \text{and } f'(\infty) = 1 \ . \tag{6.3b}$$

While one can not write down the function f exactly it is a simple matter to solve the ODE (6.3a,b) numerically with great accuracy (White [31], p. 262) thus obtaining an effectively exact solution.

Blasius flow is a solution of equations (1.1a-e) over the semi-infinite flat plate, $0 < x < \infty$, $0 \leq y < \infty$. There is a small neighborhood of the leading edge of the plate in which the transverse velocity component is of the same order of magnitude as the tangential velocity component. The Prandtl equations are therefore not valid in this region. In order to ameliorate the effects of this leading edge singularity and in order to conveniently handle the right hand boundary of our computational domain we consider the following periodic problem.

We compute over the portion of the plate from $a = 3h$ to $b = 1 + 3h$. We map physical space, $\Omega \equiv \{(x, y) : x > 0, \text{ and } y \geq 0\}$, onto the periodic domain $\Omega_C \equiv \{(x, y) : 3h \leq x \leq 1 + 3h, \text{ and } y \geq 0\}$ (C for 'computational') by the transformation $(x, y) \in \Omega \rightarrow (x^*, y^*) \in \Omega_C$ where

$$x^* = x \ mod \ 1 \tag{6.4a}$$

$$y^* = y \sqrt{x^*/x} \ . \tag{6.4b}$$

Sheets which move to the right of $x = b$ have their centers transformed according to (6.4a,b) so that they now appear to lie near the beginning of Ω_C. Similarly, sheets which move backwards, to the left of $x = a$, are rescaled and placed at the end of Ω_C. Furthermore, when calculating the velocity of a point that lies within one sheet length of the edge of our computational domain we take care to include the influence of sheets which lie near the other end.†

In this way we eliminate the effects of the leading edge singularity by imposing as an upstream boundary condition the computed velocity profile that results from identifying $x = a$ and $x = b$ with appropriately scaled y coordinates. This also eliminates spurious effects due to throwing sheets away after they pass $x = b$ (see Chorin [9], p. 433).

One drawback of the periodic formulation of this problem is that one never throws away sheets. Once a sheet is created it exists for the remainder of the computer calculation. Since the no-slip boundary condition is frequently violated at the end of the advection step, it follows that the total number of vortex elements in the flow increases with time. For Blasius flow this is non-physical. It is our contention, however, that this is a good test of the algorithm's effectiveness. Vorticity creation is an important phenomenon and one would like to approximate it as accurately as possible. Successful strategies for minimizing the error in the vorticity creation algorithm will lead to a better overall algorithm. Furthermore, the error estimates

† I am indebted to Jim Shearer for suggesting this formulation of the Blasius problem.

obtained for the periodic flow will presumably be worse than errors measured for flows in which sheets are thrown away, and therefore constitute an upper bound on the error in computing Blasius flow with the vortex sheet method.

All the computer runs reported on in this paper were run with $\nu = 10^{-4}$ and with initial data

$$u^0(x,y) = \begin{cases} 1, & y > 0, \\ 0, & y = 0. \end{cases} \tag{6.5}$$

All results are measured at time $T = 2.0$

6.2. Measurement of the Error In order to eliminate the dependence of the integral L^p norm of the error on the viscosity (see §5.2) we measure all such norms in the transformed variables (x,η),

$$\| u - \tilde{u} \|_p = \left(\int_a^b \int_0^\infty | u(x,\eta) - \tilde{u}(x,\eta) |^p \, d\eta \, dx \right)^{\frac{1}{p}} \tag{6.8}$$

where η is given by (6.2). Furthermore, when $p = 1$ we divide the error in the L^1 norm by

$$\| 1 - u \|_1 = \int_a^b \int_0^\infty (1 - f'(\eta)) d\eta \, dx = (\eta - f(\eta)) \Big|_{\eta=0}^{\eta=\infty} \approx 1.7208$$

(see [24], p. 130) and report the 'normalized' error,

$$\| u - \tilde{u} \|_1 / \| 1 - u \|_1 . \tag{6.9}$$

To estimate the integral norm in (6.8) we used

$$\| u - \tilde{u} \|_p \approx \left(\sum_{i=1}^{r} h \int_0^\infty | u(a_i, \eta) - \tilde{u}(a_i, \eta) |^p \, d\eta \right)^{\frac{1}{p}}$$

$$= h^{\frac{1}{p}} \left(\sum_{i=1}^{r} (\sqrt{\nu a_i})^{-1} \int_0^\infty | u(a_i, y) - \tilde{u}(a_i, y) |^p \, dy dx \right)^{\frac{1}{p}} .$$

The one dimensional error above a_i was calculated using the trapezoid rule

$$\int_0^\infty | u(a_i, y) - \tilde{u}(a_i, y) |^p \, dy \approx \sum_j ((err_j)^p + (err_{j+1})^p)(y_{j+1} - y_j)/2 \tag{6.10}$$

where $err_j = | u(a_i, y_j) - \tilde{u}(a_i, y_j) |$, the sum is only over those y_j such that

$$b_h(a_i - x_j) \neq 0, \tag{6.11}$$

and we have ordered the y_j so that $y_j \leq y_{j+1}$ for all j. i.e., we use a grid that corresponds to the location of the sheets above a_i. To ensure that the sum in (6.10) starts at $y = 0$ we place an sheet with no weight at $(a_i, 0)$. The value of $u(a_i, y_j) = f'(y_j / \sqrt{\nu a_i})$ was determined by linear interpolation from an array containing values of f' at equally spaced points η=0.0, 0.01, . . . , 8.0. We estimate the sup norm of the error similarly,

$$\| u - \tilde{u} \|_\infty \approx \max\{ | u(a_i, y_j) - \tilde{u}(a_i, y_j) | \},$$

where the max is taken over all i, j satisfying (6.11).

The velocity, vorticity, drag, and each of the various norms of the error are random variables. We therefore made several different runs (which we refer to as *trials*) each with a different starting seed for the random number generator. We estimate the expected value of a randomly varying quantity, Θ, by $\overline{\Theta}$ where

$$\overline{\Theta} = \frac{1}{n} \sum_{i=1}^{n} \Theta_i \tag{6.12}$$

and Θ_i is the value of Θ calculated from the ith trial. We estimate the standard deviation of Θ by

$$\tilde{\sigma} \approx \frac{1}{\sqrt{n-1}} \left(\sum_{i=1}^{n} (\Theta_i - \overline{\Theta})^2 \right)^{\frac{1}{2}} . \tag{6.13}$$

It is useful to consider the *standard error*, σ_Θ, of the estimate in (6.12) defined by

$$\sigma_\Theta \equiv \frac{\sigma}{\sqrt{n}} \tag{6.14}$$

where σ is the true standard deviation for the parent distribution of the Θ_i. The quantity σ_Θ is simply the standard deviation of the distribution of the $\overline{\Theta}$'s and is therefore a measure of how good an estimate (6.12) is of the true mean. (See [18], p. 21.) Since we do not know σ we will use (6.14) with σ replaced by $\tilde{\sigma}$ from (6.13). Unless noted otherwise, all of the data below are estimates based on $n = 25$ trials.

6.3. An Estimate of the Rate of Convergence We begin by presenting numerical results which demonstrate the convergence of the vortex sheet method in the case of Blasius flow and from which we can estimate the rate of convergence. Table 1 contains the discrete L^1 norm of the error (normalized as in (6.9)) at time $T = 2$. In Table 2 we present the standard deviation of these errors obtained with formula (6.13). Note that the standard deviation decreases along both rows and columns.

It is apparent that for all values of $\omega_{\max}$ the error decreases with decreasing h as long as $h < \omega_{\max}$ but levels off or begins to increase as h approaches $\omega_{\max}$. We observed this phenomenon consistently in all of our runs. It was particularly pronounced when B-spline smoothing was used. We find it surprising that the standard deviation decreases even while this error grows. We will investigate this behavior more thoroughly in §6.6 below.

A Study of the Convergence Rate in the L^1 Norm as a Function of ω_{max}

	h $(\Delta t = h)$				
ω_{max}	0.2	0.1	0.05	0.025	0.0125
0.2	0.4002	-	-	-	-
0.1	0.2989	0.2983	-	-	-
0.05	0.2580	0.2239	0.2230	-	-
0.025	0.2663	0.1773	0.1657	0.1903	-
0.0125	0.2483	0.1636	0.1267	0.1346	0.1864
0.00625	0.2529	0.1594	0.1088	0.0990	0.1159†
0.003125	0.2473	0.1528	0.1007	0.0778†	-
0.0015625	0.2511	0.1534	0.0857†	0.0669‡	-

Table 1 Piecewise Linear Cutoff

The Standard Deviation of the Errors in Table 1

	h $(\Delta t = h)$				
ω_{max}	0.2	0.1	0.05	0.025	0.0125
0.2	0.0734	-	-	-	-
0.1	0.0638	0.0521	-	-	-
0.05	0.0475	0.0399	0.0279	-	-
0.025	0.0473	0.0239	0.0112	0.0165	-
0.0125	0.0243	0.0202	0.0126	0.0101	0.0069
0.00625	0.0252	0.0104	0.0103	0.0075	0.0060†
0.003125	0.0146	0.0093	0.0069	0.0077†	-
0.0015625	0.0088	0.0068	0.0078†	-	-

Table 2 Piecewise Linear Cutoff

We repeated this experiment with the time step halved ($\Delta t = h/2$) in an effort to determine if any of the errors would decrease as Δt decreased. These errors, presented in Table 3, were remarkably close to the previous results, sometimes agreeing to several decimal places. Furthermore, most of these new errors lie within two standard errors of the figures in Table 1 (using the estimates of the standard deviation from Table 2), making the two quantities statistically indistinguishable from each other. This was also true for the errors in the L^2 norm. Thus we conclude that the errors presented in Table 1 do not vary 'independently' with the time step

† Here $5 \leq n < 25$ where n is the number of trials.

‡ $n = 1$.

in the sense that they do not diminish when h and ω_{max} are fixed and Δt decreased. This may well be due to the fact that we are computing a stationary flow.

The Errors are Independent of Δt .

	h $(\Delta t = h/2)$				
ω_{max}	0.2	0.1	0.05	0.025	0.0125
0.2	0.4318	-	-	-	-
0.1	0.3215	0.2967	-	-	-
0.05	0.2762	0.2336	0.2463	-	-
0.025	0.2721	0.1787	0.1778	0.2170	-
0.0125	0.2402	0.1586	0.1276	0.1498	0.2146†

Table 3 Piecewise Linear Cutoff

Returning to Table 1 we note that for small, fixed ω_{max} the errors decrease like $h^{2/3}$. We conjecture that there are two sources of error which depend predominantly on h, one like $O(h^{2/3})$ and another which grows if h tends to zero much faster than ω_{max}. Hence, for $\omega_{max} << h$ the first error dominates and we find the errors that behave like $O(h^{2/3})$. On the other hand, as we shall document in §6.6 below, when h decreases faster than ω_{max} the second source begins to dominate and we observe gradually increasing errors. We speculate that this second source of error may be due to the fact that

$$\partial_x \; \omega_j \; b_h(x - x_j) = O(\omega_{max}/h) \; .$$

In other words, sheets induce local (non-physical) fluctuations in the velocity (and vorticity) which are $O(\omega_{max}/h)$ as one moves in the direction parallel to the wall. The exact cause of these sources of error and the nature of their dependence on the parameters remains an open question.

Note that as one moves vertically down a column the error eventually levels out. This 'plateau' is due to sources of error, such as the splitting error, which are unaffected by ω_{max}.

† $n = 5$

Since Δt and h are constant along columns it follows that any decrease in the error along columns is due to $\omega_{\max}$ alone.

It is difficult to obtain a precise estimate of the rate at which the error depends on $\omega_{\max}$ We believe this rate to be $O(\omega_{\max}{}^{\alpha})$ for some $1/3 \leq \alpha \leq 1/2$. We choose a lower bound of 1/3 based on (4.22) and the data presented here. Furthermore, we believe it is very likely that $\alpha = 1/2$. In [23] Roberts showed that for the random vortex method the error deceases like $\sqrt{N}^{-1}$ where N is the number of vortices used. This corresponds to a rate of $\sqrt{\omega_{\max}}$ for the vortex sheet method. In contrast, the theoretical bounds for the random vortex method in [14] only predict a rate of $\log N / \sqrt[4]{N}$ in the L^2 norm. Similar remarks apply to the bounds established in [21] on the random gradient solution of the Kolmogorov equation.

All of our numerical experiments were made under the assumption that the error was $O(\sqrt{\omega_{\max}})$. The danger in assuming a rate slower than the true one is that we end up doing more work than necessary to achieve a given level of accuracy. The danger in assuming a rate which is faster than the true one is that we may end up in a regime in which errors result from too rapid a decrease of the parameter h.

A Convergence Study with $h = O(\omega_{\max}{}^{3/4})$ *and* $\Delta t = h$.

	($\Delta t = h$)						
$\omega_{\max}$	L^1 norm	L^2 norm	L^∞ norm	sheets	time	$\delta_1$av	$\delta_2$av
0.025	0.2817	0.2489	0.2708	226	0.002	0.0044	0.00161
0.0125	0.1617	0.1756	0.2677	939	0.022	0.0024	0.00070
0.00625	0.1044	0.1070	0.1536	2954	0.218	0.0013	0.00037
0.003125	0.0823	0.0915	0.2719	13755	3.638	0.0009	0.00029
0.0015625	0.0592	0.0631	0.1141	37206	31.131	0.0007	0.00019

Table 4 (1 trial per row)

We made a sequence of runs with $\omega_{\max}^{1/2} = O(h^{2/3})$. The results appear in Table 4. We started with $\omega_{\max} = 0.025$ and $h = 0.2$ and decreased $\omega_{\max}$ by 2 while decreasing h by $2^{3/4}$. As before we take $\Delta t = h$. Note that each row of data is from only one trial.

The column labeled 'time' contains the time, in minutes, it took for 1 trial on a CRAY X-MP. The FORTRAN program was designed to be as fast as possible. In particular, we vectorized every loop that would admit vectorization. We also employed a 'bin' data structure in which all sheets lying in $a_i - h/2 \leq x < a_i + h/2$ are kept in the same bin. Thus, in order to compute the velocity of a sheet in the ith bin we need only loop over those sheets in adjacent bins. Thus, in the advection step, instead of every sheet interacting with every other for a total of N^2 interactions each sheet has approximately $(2R+1)hN$ interactions where R is as in (2.8b). This results in an algorithm which is

$$O((2R+1)\, h\ N^2)\ . \tag{6.15}$$

The column labeled $\delta_1 av$ is the average error in the *displacement thickness* defined by

$$\delta_1 av = \frac{1}{r} \sum_{i=1}^{r} |\, \delta_1(a_i) - \tilde{\delta}_1(a_i)\, |\ . \tag{6.16}$$

Here $\delta_1(a_i)$ is the displacement thickness above a_i,

$$\delta_1(x) = \int_0^\infty (1 - \frac{u(x,y)}{U(x)})\, dy$$

(Schlichting [24], p. 140) and $\tilde{\delta}_1$ is the trapezoid rule approximation to δ_1 given by (6.10) with $u(a_i, y)$ replaced by 1. Similarly, $\delta_2 av$ is the average error in the momentum thickness defined by (6.16) with δ_1 and $\tilde{\delta}_1$ replaced by δ_2 and $\tilde{\delta}_2$ where

$$\delta_2(x) = \int_0^\infty \frac{u(x,y)}{U(x)}(1 - \frac{u(x,y)}{U(x)})\ dy\ .$$

(Schlichting [24], p. 141) and $\tilde{\delta}_2$ is the trapezoid rule approximation to δ_2. Note that we have not scaled out the effect of ν in our calculation of $\tilde{\delta}_1$ and $\tilde{\delta}_2$. Thus $\delta_1 av$ and $\delta_2 av$ are $O(\sqrt{\nu}) = O(10^{-2})$.

We chose ω_{max}/h small in order to compute in a regime with small variance. We wished to demonstrate that one need not average in order to effectively use these random walk methods. The fact that most of the results reported on in this paper are averages should not be construed as suggesting that one must always 'ensemble average' to get reasonable results. It is sufficient to make one run as long as it is in a regime of small variance.† In particular, note that the errors in the L^1 and L^2 norms as well as the average errors in momentum and displacement thickness decrease at the anticipated rate of $1/\sqrt{2}$ without averaging. The L^∞ norm was not as well behaved, an issue which we shall pursue no further.

It should be remarked that Blasius flow is not only a stationary solution of the Prandtl equations but a similarity solution as well. Therefore, these results may not be representative of what happens with more general flows.

6.4. Second Order Integration in Time In order to determine the effect of solving (2.17a,b) with a higher order ODE solver we conducted the same experiment as in Table 1 but with the movement of the sheets in the advection step now being given by

$$x_j^{k+1/2} = x_j^k + \Delta t \ \tilde{u}_{1/2}(x_j', y_j')$$

$$y_j^{k+1/2} = y_j^k + \Delta t \ \tilde{v}_{1/2}(x_j', y_j')$$

where

$$x_j' = x_j + \frac{1}{2} \Delta t \ \tilde{u}^k(x_j^k, y_j^k)$$

$$y_j' = y_j + \frac{1}{2} \Delta t \ \tilde{v}^k(x_j^k, y_j^k)$$

† Thus, for small ν, 1 trial should be sufficient even though the values of the other computational parameters may be large. For example, see [6].

is the position of the jth sheet after one half of a time step and $(\tilde{u}_{1/2}, \tilde{v}_{1/2})$ is the velocity field induced by the sheets when their centers are at these positions.

Second Order Integration in Time

	h $(\Delta t = h)$				
ω_{max}	0.2	0.1	0.05	0.025	0.0125
0.2	0.4224	-	-	-	-
0.1	0.3290	0.3183	-	-	-
0.05	0.2736	0.2316	0.2547	-	-
0.025	0.2261	0.1701	0.1759	0.2271	-
0.0125	0.2325	0.1552	0.1325	0.1531†	0.2239†

Table 5 Piecewise Linear Cutoff

Comparing these results with Table 1 we observe no increase in accuracy over the Euler's method solution of (2.17a,b). Furthermore, we noticed a marked increase in the rate at which the number of sheets in the flow grew as h was decreased with ω_{max} left fixed. Of course here we did not use Strang splitting and hence do not expect to see all sources of error that depend on Δt decrease. Nonetheless, unlike the results in Table 2 of [21], here there appears to be no improvement in the error due to second order time discretization.

There seems to be a prevalence of opinion among users of hybrid vortex sheet/vortex blob methods that the use of a higher order time integration will result in a better solution. (For example, [6, 29, 30].) Perhaps this opinion is based on theoretical results for the vortex method solution of the Euler equations with higher order time integration ([1, 17]). However, the following points should be made with regards to the vortex sheet method. A second order scheme such as the one used here results in twice as much work. Furthermore, we are constrained by (5.2) to decrease Δt as rapidly as h. Our results indicate that the dominant sources of error are those that depend on h and ω_{max}. Hence one may be doing twice as much work for a negligible gain in accuracy. We suspect these considerations may apply to other flows as well.

† $5 \leq n < 25$

We remark that Tiemroth [30] used a second order time integration in conjunction with Strang splitting and reports improved results. We tried this approach in our numerical experiments with the random gradient solution of the Kolmogorov equation and also observed improvements. However, to achieve the full benefit of the higher order time integration and higher order splitting one needs to balance the $O(\Delta t^2)$ errors with the other sources of error. Since we know of no way to increase the rate that the error decreases with h and ω_{max} we question the wisdom of computing the velocity field twice as often in order to diminish only one source of error.

6.5. B-Spline Smoothing In Table 6 below we present the average of the error in the L^1 norm versus the average number of sheets at time $T = 2.0$ for the vortex sheet method with the B-spline cutoff. These figures should be compared with Table 7 which contains the same data for the piecewise linear cutoff. The two methods achieved comparable levels of accuracy. Furthermore, for some values of ω_{max} and h spline smoothing results in fewer sheets.

L^1 Norm of the Error versus Number of Sheets with $\Delta t = h$

	h $(\Delta t = h)$					
ω_{max}	0.2		0.1		0.05	
	sheets	error	sheets	error	sheets	error
12^{-1}	52	0.3162	144	0.3099	511	0.3769
24^{-1}	105	0.2514	285	0.2173	973	0.2775
48^{-1}	198	0.2460	526	0.1632	1686	0.1864
96^{-1}	390	0.2130	960	0.1467	2851	0.1245
192^{-1}	746	0.2328	1778	0.1346	4923	0.0989
384^{-1}	1455	0.2200	3332	0.1346	8676	0.0857
768^{-1}	2894	0.2411†	6033	0.1485†	14831	0.0928†
1536^{-1}	5694	0.2178†	12064	0.1312†	28167	0.0677†

Table 6 B-spline Cutoff

† $n = 1$

For a given combination of h, $\omega_{\max}$, and Δt let N_S be the number of sheets created with spline smoothing and let N_P denote the number of sheets created with piecewise linear smoothing. Table 8 contains the ratio N_S/N_P as a function of the parameters. It is apparent that this ratio grows with increasing $\omega_{\max}/h$, eventually becoming greater than 1. It appears that one might be able to keep the ratio N_S/N_P constant by decreasing $\omega_{\max}$ three or four times as fast as h. However this is much faster than we concluded was necessary above. Perhaps this is due to a faster rate of convergence as a function of h for the splines. We note that if the B-spline algorithm was $O(h^{4/3})$ then the rate at which one must decrease h relative to $\omega_{\max}$ in order to balance $O(h^{4/3}) = O(\omega_{\max}^{1/2})$ is roughly the same rate that appears to result in a constant N_S/N_P.

L^1 Norm of the Error with $\Delta t = h$

	h $(\Delta t = h)$					
$\omega_{\max}$	0.2		0.1		0.05	
	sheets	error	sheets	error	sheets	error
12^{-1}	64	0.2902	152	0.2725	387	0.2923
24^{-1}	131	0.2471	302	0.1919	764	0.2137
48^{-1}	264	0.2358	595	0.1572	1475	0.1529
96^{-1}	519	0.2127	1144	0.1442	2768	0.1130
192^{-1}	1027	0.2207	2217	0.1382	5203	0.0911
384^{-1}	2025	0.2201	4319	0.1315	9690	0.0811
768^{-1}	4017	0.2290†	8471	0.1354†	18521	0.0865†
1536^{-1}	8016	0.2304†	16523	0.1373†	35240	0.0779†

Table 7 Piecewise Linear Cutoff

The relationship between the growth of the error, the increase in the ratio N_S/N_P, and the rate at which $\omega_{\max}$ is reduced relative to h merits further study. We find it puzzling that presumably more accurate methods, second order Runge-Kutta above and spline interpolation here, result in an increased rate of growth, in both the sheets and the errors, when h is diminished with fixed $\omega_{\max}$.

† $n = 1$

Until a more complete understanding of this phenomenon is forthcoming we feel that some care should be taken with the B-spline smoothing. We suggest making (small) runs with each smoothing, using several different choices of $\omega_{\max}$ and h, and plotting the ratio N_S/N_P. One can then extrapolate to find the proper combinations of $\omega_{\max}$ and h for large runs. In fact, this may be a way to find combinations of $\omega_{\max}$ and h for which the variance is small.

The ratio N_S/N_P.

	h ($\Delta t = h$)		
$\omega_{\max}$	0.2	0.1	0.05
12^{-1}	0.81	0.95	1.32
24^{-1}	0.80	0.94	1.27
48^{-1}	0.75	0.88	1.14
96^{-1}	0.75	0.84	1.03
192^{-1}	0.73	0.80	0.95
384^{-1}	0.72	0.77	0.90
768^{-1}	$0.72^{\dagger}$	$0.71^{\dagger}$	$0.80^{\dagger}$
1536^{-1}	$0.71^{\dagger}$	$0.73^{\dagger}$	$0.80^{\dagger}$

Table 8

The savings in computational cost due to the reduced number of sheets needs to be weighed against the increased expense of computing with B-splines. The cutoff in (3.4) is moderately more expensive to evaluate than that in (3.2). Furthermore, since the support of the B-spline cutoff is twice as large as that of the piecewise linear cutoff the number of sheets needed to evaluate the velocity in (see (6.15)) roughly doubles. On the other hand, when the vortex sheet method is combined with a vortex method solution of the Navier-Stokes equations, in which the sheets become vortex blobs, reducing the number of sheets by 25% may reduce the amount of work in the vortex method by 43%, i.e. roughly one half. Here we have assumed that the work in computing the velocity field in the vortex method is $O(N^2)$. In some cases this may be reduced ([2, 3, 15]).

---

† $n = 1$.

6.6. The Behavior of the Algorithm with Decreasing h Observe that the number of sheets above x is governed by $\omega_{\max}$. For example, assume that $\omega_{\max}$ divides 1 evenly and let the initial data be given by (6.5). Let N_x denote the number of sheets above x. Then at the first time step, with piecewise linear smoothing, we have

$$N_{\alpha_i} = \omega_{\max}^{-1} \qquad\qquad i = 1, \ . \ . \ . \ , r.$$

In general, at least for reasonable pressure gradients (UU_x small), one expects that

$$N_x = O(\omega_{\max}^{-1})$$

for any x.

In Table 9 we show the average number of sheets in the flow at time $T = 2.0$ as a function of $\omega_{\max}$, h, and Δt with the piecewise linear smoothing. It is apparent that if one fixes h and Δt and decreases $\omega_{\max}$ by 2 that, on the average, the number of sheets above x roughly doubles. In fact, if we restrict ourselves to regions for which $\omega_{\max} < h$ it is rare for the number of sheets to more than double. (Some of the figures here differ from those in Table 1 even though the choice of parameters is the same. This is due to the fact that these trials were made on a different computer with a different random number generator.)

Gradual Increase of the L^1 Error for Decreasing h, Δt and Fixed $\omega_{\max}$

	h ($\Delta t = h$)							
$\omega_{\max}$	0.2		0.1		0.05		0.025	
	sheets	error	sheets	error	sheets	error	sheets	error
0.2	26	0.4317	63	0.4449	179	0.5434	880	0.6860
0.1	54	0.3106	125	0.2915	328	0.3331	1074	0.4169
0.05	109	0.2724	253	0.2054	641	0.2317	1986	0.2858
0.025	222	0.2524	498	0.1681	1248	0.1630	3702	0.1989

Table 9 Piecewise Linear Cutoff

One would also expect that letting h go to $h/2$ would produce similar results. This turns out not to be the case. It is apparent from Tables 6 and 9 that the (average) number of sheets

in the flow always increases by *more* than 2, often by much more. Since in all these runs $\Delta t = h$, one can inquire if this unexpected increase is due to the increased number of time steps. To answer this question we made a sequence of runs fixing $\Delta t = 0.0125$ and reducing h as before. The results appear in Table 10. It is apparent that the errors continue to grow as h decreases with ω_{max} fixed. Therefore this phenomenon is not due to decreasing Δt.

In all but one case the errors in Table 10 are larger than those in Table 9. The same is true for the number of sheets. In some cases, particularly in the last column, the difference is by as much as 7 standard errors. Provided our estimate of the standard error is reasonably accurate, this is statistically significant. It seems to run counter to our intuition that the errors should be worse for a smaller time step. We can offer no explanation. We do note however that an abnormal growth in the number of sheets seems to characterize these regions of parameter space that produce large errors.

Gradual Increase of the L^1 Error for Decreasing h and Fixed Δt, ω_{max}

	h ($\Delta t = 0.0125$)							
ω_{max}	0.2		0.1		0.05		0.025	
	sheets	error	sheets	error	sheets	error	sheets	error
0.2	31	0.4380	79	0.4489	242	0.5339	1056	0.7514
0.1	64	0.3640	158	0.3110	451	0.3647	1427	0.4549
0.05	128	0.2849	320	0.2310	909	0.2549	2745	0.3228
0.025	246	0.2733	612	0.1789	1712	0.1839	4978	0.2167

Table 10

We consider this phenomenon important for the several reasons. The amount of work to compute the velocity at each of the sheets in the advection step is either $O(N^2)$ or, with a bin data structure, $O(hN^2)$ where N is the total number of sheets in the flow. Thus, reducing h by 2 results in a greater increase in computational cost than reducing ω_{max} by 2. Furthermore, errors eventually begin to grow if h is decreased with ω_{max} left fixed. In particular, these observations together with (4.23) imply that the vorticity in the flow will remain constant if h and Δt are fixed and ω_{max} is decreased but grow if h and Δt are decreased with ω_{max} fixed. Conse-

quently, the bounds in §4.2 worsen. Unfortunately, one cannot pursue a strategy of only decreasing ω_{max}, for eventually there is no improvement except possibly a reduction in the variance. One must therefore toe a fine line between decreasing h too rapidly and not decreasing h fast enough.

6.7. A Comparison of Particle Creation Algorithms In this section we present the results of a numerical experiment designed to compare the two particle creation algorithms described in §2.3.2. We obtained the errors in Table 11 with creation Algorithm A using a value of $\omega_{min} = 10^{-6}$. Table 12 is a duplicate of Table 11 except here we used the creation Algorithm B. i.e., the same algorithm used for all other experiments in this paper. Note that here the errors are in the discrete L^2 norm.

Discrete L^2 Norm of the Error

	h $(\Delta t = h)$							
ω_{max}	0.2		0.1		0.05		0.025	
	sheets	error	sheets	error	sheets	error	sheets	error
0.2	60	0.3600	-	-	-	-	-	-
0.1	88	0.2957	289	0.2738	-	-	-	-
0.05	145	0.2525	427	0.2103	1407	0.2416	-	-
0.025	255	0.2327	676	0.1783	2021	0.1690	7076	0.2310†
0.0125	477	0.2021	1150	0.1400	3109	0.1164	9860	0.1350†

Table 11 Algorithm A

It is apparent that Algorithm A results in an increase in the number of sheets in the flow but with little or no improvement in accuracy. We also tried replacing $\omega_{min} = 10^{-1}$ with $\omega_{min} = \omega_{max}/2$ and observed a similar result: no noticeable improvement in the error but more sheets than Algorithm B. Thus, we conclude that Algorithm A results in no observable increase in accuracy but leads to a greater computational cost.

† $10 \leq n < 20$

Discrete L^2 Norm of the Error

	h $(\Delta t = h)$							
ω_{max}	0.2		0.1		0.05		0.025	
	sheets	error	sheets	error	sheets	error	sheets	error
0.2	27	0.3610	-	-	-	-	-	-
0.1	53	0.2763	124	0.2766	-	-	-	-
0.05	109	0.2410	251	0.2090	638	0.2087	-	-
0.025	216	0.2378	495	0.1709	1256	0.1612	3749	0.1808
0.0125	430	0.2222	972	0.1549	2370	0.1258	6775	0.1329

Table 12 Algorithm B

6.8. Sheet Tagging Finally we made a run with the same values of parameters as in Table 12 but this time using sheet tagging. We present the L^1 norm of the error and it's variance in Table 13. These figures may be compared with Tables 1 and 2. It is apparent that the sheet tagging leads to neither a decrease in the error nor a reduction of the variance. We remain very dubious about the use of sheet tags.

Discrete L^1 Norm of the Error

	h $(\Delta t = h)$							
ω_{max}	0.2		0.1		0.05		0.025	
	error	$\tilde{\sigma}$	error	$\tilde{\sigma}$	error	$\tilde{\sigma}$	error	$\tilde{\sigma}$
0.2	0.5508	0.2671	-	-	-	-	-	-
0.1	0.4574	0.1933	0.3677	0.1938	-	-	-	-
0.05	0.2922	0.1145	0.2524	0.0748	0.2844	0.0777	-	-
0.025	0.2422	0.1236	0.1729	0.0399	0.2026	0.0437	0.2045	0.0236
0.0125	0.2406	0.0893	0.1638	0.0637	0.1413	0.0308	0.1490	0.0179

Table 13 Sheet Tagging

6.9. Conclusions In the case of Blasius flow we conclude that for fixed ν, $\Delta t \leq h$, and $\omega_{max} < h$ the vortex sheet method converges like $O(\sqrt{\omega_{max}}) + O(h^{2/3})$. However, if h is allowed to decrease much faster than ω_{max} the error eventually begins to grow. We have also shown that for $1 \leq p < \infty$ the error in the L^p norm decreases like $\nu^{1/2p}$.

Our investigation of the algorithm when h tends to 0 much faster than ω_{max} has shown that the increasing errors are accompanied by an increased growth rate in the number of sheets. This leads to a rapid increase in the computational cost of the algorithm. Thus, in order to ensure that the errors will decrease as the parameters tend to 0, we recommend setting $\Delta t \leq h$ and $h = O(\omega_{max}{}^{3/4})$.

Experiments with B-spline smoothing indicate that for the same choice of parameters the error is comparable to that obtained with piecewise linear smoothing. Additionally, we were able to diminish the number of sheets created by as much as 25% through the use of the B-splines. However this reduction was only evident for certain choices of the parameters. It appears that to ensure a 25% reduction in the number of sheets h and ω_{max} must be chosen so that ω_{max} decreases three or four times as fast as h. Further work is necessary to determine if the splines are indeed a viable improvement to the vortex sheet method.

We have also demonstrated that a more cost efficient algorithm results when all sheet strengths are chosen to have magnitude ω_{max}. Finally, on the basis of numerical evidence presented here, we conclude that the variance reduction technique known as sheet tagging introduced in [9] is of questionable value.

References

1. C. R. Anderson and C. A. Greengard, "On Vortex Methods," *Siam J. Numer. Anal.*, vol. 22, 1985.

2. C. R. Anderson, "A Method of Local Corrections for Computing the Velocity Field Due to a Distribution of Vortex Blobs," *J. Comp. Phys.*, vol. 62, pp. 111-123, 1986.

3. S. Baden, "Dynamic Load Balancing of a Vortex Calculation Running on Multiprocessors," *Lawrence Berkeley Laboratory preprint*, no. 22584, 1987.

4. Carl de Boor, *A Practical Guide to Splines*, Springer-Verlag, New York, 1978.

5. A. Y. Cheer, "A Study of Incompressible 2-D Vortex Flow Past a Circular Cylinder," *SIAM J. Sci. Stat. Comput.*, vol. 4, pp. 685-705, 1983.

6. A. Y. Cheer, "Unsteady Separated Wake Behind an Impulsively Started Cylinder in Slightly Viscous Fluid," *manuscript*, U. C. Davis, 1986.

7. Y. Choi, J. A. C. Humphrey, and F. S. Sherman, "Random Vortex Simulation of Transient Wall-Driven Flow in a Rectangular Enclosure," *submitted to J. C. P.*, 1986.

8. A. J. Chorin, "Numerical Study of Slightly Viscous Flow," *J. Fluid Mech.*, vol. 57, pp. 785-796, 1973.

9. A. J. Chorin, "Vortex Sheet Approximation of Boundary Layers," *J. Comp. Phys.*, vol. 27, pp. 428-442, 1978.

10. A. J. Chorin and J. E. Marsden, *A Mathematical Introduction to Fluid Mechanics*, Springer-Verlag, New York, 1979.

11. A. J. Chorin, "Vortex Models and Boundary Layer Instability," *SIAM J. Sci. Stat. Comput.*, vol. 1, pp. 1-21, 1980.

12. W. Feller, "An Introduction to Probability Theory and Its Applications," *2nd ed.*, vol. II, John Wiley & Sons, New York, 1971.

13. A. F. Ghoniem, A. J. Chorin, and A. K. Oppenheim, "Numerical Modeling of Turbulent Flow in a Combustion Tunnel," *Philos. Trans. Roy. Soc. London*, vol. A304, pp. 303-325, 1982.

14. J. Goodman, "Convergence of the Random Vortex Method in Two Dimensions," *Comm Pure and Applied Math*, to appear.

15. L. Greengard and V. Rokhlin, "A Fast Algorithm for Particle Simulations," *Yale Research Report*, YALEU/DCS/RR-459, 1986.

16. O. H. Hald, "Convergence of a Random Method With Creation of Vorticity," *Siam J. Sci. Stat. Comput.*, vol. 7 , pp. 1373-1386, 1986.

17. O. H. Hald, "Convergence of Vortex Methods for Euler's Equations, III," *Siam J. Num. Analysis*, to appear.

18. J. M. Hammersley and D. C. Handscomb, *Monte Carlo Methods*, Methuen & Co. Ltd, London, 1964.

19. F. John, *Partial Differential Equations*, Springer Verlag, 1982.

20. L. D. Landau and E. M. Lifshitz, *Fluid Mechanics*, Pergamon Press, New York, 1959.

21. E. G. Puckett, "Convergence of a Random Particle Method to Solutions of the Kolmogorov Equation," *Lawrence Berkeley Laboratory Preprint*, no. 22420, 1987.

22. S. G. Roberts, "Convergence of a Random Walk Method for Burgers' Equation," *Ph.D. Thesis*, University of California, Berkeley, 1985.

23. S. G. Roberts, "Accuracy of the Random Vortex Method for a Problem with Non-Smooth Initial Conditions," *J. Comp. Phys.* , vol. 58, pp. 29-43, 1985.

24. H. Schlichting, *Boundary-Layer Theory,* McGraw-Hill, New York, 1968.

25. M. H. Schultz, *Spline Analysis,* Prentice-Hall, Inc., Englewood Cliffs, N.J., 1973.

26. J. Serrin, *Proc. Roy. Soc.*, vol. A 299, p. 491, 1967.

27. J. A. Sethian, "Turbulent Combustion in Open and Closed Vessels," *J. Comp. Phys.*, vol. 55, pp. 425-456, 1984.

28. J. A. Sethian, "Vortex Methods and Turbulent Combustion," in *Lectures in Applied Mathematics,* vol. 22, Springer Verlag, New York, 1985.

29. J. A. Sethian and A. F. Ghoniem, "Validation Study of Vortex Methods:," *J. Comp. Phys.* , to appear.

30. E. Tiemroth, "The Simulation of the Viscous Flow Around a Cylinder by the Random Vortx Method," *Ph. D. Thesis,* U. C. Berkeley, 1986.

31. F. M. White, *Viscous Fluid Flow,* McGraw-Hill, New York, 1974.

LAWRENCE BERKELEY LABORATORY
TECHNICAL INFORMATION DEPARTMENT
UNIVERSITY OF CALIFORNIA
BERKELEY, CALIFORNIA 94720